BU
ARPA-E-59


Division of Engineering
BROWN UNIVERSITY
PROVIDENCE, R. I.


# THE FLOW BEHAVIOR OF SAND AT FAILURE


J. B. WEIDLER


AD678756


20060110160



Advanced Research Projects Agency
Department of Defense
Contract SD-86
Materials Research Program

ARPA E59

August 1968

# THE FLOW BEHAVIOR OF SAND AT FAILURE

by

Jay B. Weidler, Jr.

Division of Engineering

Brown University

Providence, Rhode Island

August, 1968

TECHNICAL LIBRARY
BLDG 313
ABERDEEN PROVING GROUND MD.
STEAP-TL

[redacted]

# THE FLOW BEHAVIOR OF SAND AT FAILURE*

by

Jay B. Weidler, Jr.[1]

ABSTRACT

Inferences regarding the character of the pointwise or material flow behavior for cohesionless soils are drawn from the results of a series of tests on a sand system. Specifically these inferences are that normality to the failure surface may be preserved for projections of the plastic strain increment vector onto planes of constant hydrostatic pressure ($\pi$-planes) and that the angular deviation from normality to the failure surface for projections of the plastic strain increment vector onto planes perpendicular to the $\pi$-plane may, as a first approximation, be considered constant. For this latter inference the variation in the approximately constant angle appears to be a linear function of the relative density of the system at failure. The apparatus used to perform the experiments was a standard direct shear device. Statistical methods were employed to establish a nest of failure envelopes in the force space of the applied tractions with a parametric dependence on the relative density at failure. Normals to these surfaces were systematically compared to their associated displacement vectors. The results of this analysis led to the inferences regarding material behavior.

---

* The research reported here was supported by ARPA Contract E-43.

[1] Assistant Professor of Engineering (Research), Brown University, Providence, R. I.

# INTRODUCTION

The history of the application of the mathematical theory of plasticity to problems in soil mechanics contains numerous examples in which an analytic form, chosen to represent the failure envelope for the material, has also been used as a yield surface. The stress-strain relations resulting from this assumption require that a certain dilatation rate be in evidence when the stress state reaches this yield surface. Experiments, however, have consistently shown smaller rates of volume change than those predicted. This anomaly has given rise to considerable theoretical conjecture about the inelastic behavior of soils, yet the necessary experiments to substantiate these hypotheses have been few. The purpose of this paper is to report the results of a series of tests designed to ascertain the nature of the flow behavior of sands at failure. Specifically it was desired to determine if any relationship existed between the direction of a normal to the failure envelope and the direction of the observed plastic flow rate vector associated with that normal.

In accomplishing this objective a somewhat irregular experimental procedure was used. The basis for this technique is more fully presented in the next section, but essentially it involves studying the phenomenon under investigation at a lower level of abstraction than the customary stress-strain level. Such a procedure requires that only the force and the corresponding displacement histories acting on the boundary of a soil system during a test be monitored in order to extract useful information about the flow behavior of sand at failure. While such a technique circumvents the difficulties associated with producing and maintaining a homogeneous state of stress and strain in a soil specimen, it has the obvious drawback that the results obtained must be regarded only as inferences to the actual behavior on the stress-strain level. Although this drawback is of serious consequence to the formulation of quantitatively predictive

constitutive relationships for the material, the paucity of experimental information in this area and the still questionable validity as to the homogenuity of stresses and strains near failure in specimens tested in more sophisticated devices indicate that the results presented here may be of interest.

The testing apparatus used in this investigation was a standard direct shear device. The soil specimen in this device is subjected to certain applied tractions on its boundaries and both these tractions and their corresponding displacements can be measured. The stress and strain states within the specimen are, however, complex and unknown. As the testing procedure for this apparatus is comparatively simple and the speed at which tests can be performed comparatively rapid, the use of the device offers a somewhat expedient method for obtaining a large quantity of data. Increasing the amount of data enhances the reliability of the inferences drawn from the analysis of the results by the use of statistical methods. While such reasoning cannot in itself justify the choice of the direct shear device, the well established observation that the force-deformation curves obtained from direct shear testing do qualitatively imitate their triaxial test counterparts offers some additional justification for its adoption in this testing program.

Conceptually the experimental program involved the establishment of a failure envelope in a hyperspace of the applied tractions and the configuration parameters of the system which best fitted the observed data. Equally, this single failure envelope may be represented as a nest of envelopes in a space of the applied tractions. Normals to this nest of failure envelopes were then systematically compared to their corresponding plastic deformation increment vectors to ascertain if any relationship existed between them at failure.

The subsequent section presents the historical background to this subject and the basis underlying the adoption of the particular investigative approach

used in this study. Succeeding sections contain a description of the experimental procedure, a discussion of the testing program, the presentation of the test results, and the analysis made of these results. Lastly the inferences obtained from the analysis are summarized and discussed. The definitions of all symbols used in the paper may be found in Appendix II. - Notation. Each symbol will be explained in the text when first used.

## HISTORICAL BACKGROUND

The application of the mathematical theory of plasticity to the problems of soil mechanics was initially made in a series of papers by Drucker and Prager (6)[2], Shield (28), Drucker (7), and Shield (29, 30). In these investigations generalizations of the Coulomb failure criterion were proposed as possible yield surfaces for the material. As pointed out by these writers and later commented on by Drucker, Gibson and Henkel (9) the use of such generalizations as possible yield surfaces places certain restrictions on the direction of the plastic strain increment vector at failure. One of these restrictions requires a certain dilatation rate to accompany a stress state on the yield surface. Hansen (13) observed that the dilatation rates predicted by plasticity theory were considerably in excess of those found in practice. This discrepancy between prediction and observation has been substantiated numerous times in the literature.

Subsequent theoretical work by Drucker et al (9), Jenike and Shield (18), Drucker (10, 12), Rowe (25, 26), Brown (4), Horne (17), Palmer (21) and this author and Paslay (31) has been directed towards the establishment of an inelastic theory which more accurately predicts the behavior of granular media and thus accomodates the aforementioned discrepancy. One of the purposes of performing the experiments reported here was to provide data which might be useful in

[2] Numbers in parentheses refer to corresponding items in Appendix I. - References.

testing the validity of these more advanced theories.

In conjunction with the analytical work mentioned above, considerable advancement has been made in the field of mechanical testing of soils. The modifications to triaxial devices and procedures by Rowe and Barden (27), Bishop and Green (2), Barden and Khayatt (1) and others represent considerable improvements towards the achievement of homogeneous states of stress and strain within the triaxial sample. Apparati devised by Kirkpatrick (19), Haythornthwaite (14), Wu, Loh, and Malvern (33) and Ko and Scott (20) have been notable advancements in the technique of applying a truly three dimensional stress field. Out of this work and the contributions of Roscoe, Schofield and Wroth (23), Roscoe, Schofield, and Thurairajah (24) and Cornforth (5) a more accurate picture of the shape of the failure envelope for granular media and its dependence on material density has emerged. Still, however, certain doubts persist as to the statical determinateness and homogeneity of the stress and strain fields within the specimens tested by these more sophisticated devices. See, for example, Haythornthwaite (15, 16) and Broms and Jamal (3). Unfortunately the greatest uncertainty exists at or near the failure of the specimen. How well the various testing devices are predicting pointwise material properties rather than system behavior in these limiting regions is still a question of some validity. As it was precisely in this neighborhood of failure that information concerning the flow behavior was sought, the experimental procedure devised for this investigation attempted to evade the issue of stresses and strains by studying the phenomenon at a lower level of abstraction.

Such a technique rests on a certain concept developed within the field of plasticity by Prager (22) and furthered by Haythornthwaite (14) and Drucker (11). Consider a material having a well defined yield surface in stress space. A two dimensional projection of this surface is shown as the convex

closed curve $f(\sigma_{ij}) = K$ in stress space $\sigma_{ij}$ of Fig. 1. If a homogeneously stressed sample of the material is tested such that the loading point moves from some point interior to the yield surface along any path to some point on the yield surface (path OY, Fig. 1) then plastic deformation ensues on reaching $\sigma_{ij}^{Y}$. Superposing the axes of a plastic strain space $\varepsilon_{ij}^{P}$ on those of the stress space $\sigma_{ij}$, the material is said to exhibit normality if the plastic strain increment vector $d\vec{\varepsilon}^{P}$ is parallel to the normal to the yield surface regardless of the location of the interior point and the path to the surface. If a system comprised of this material and loaded by an arbitrary number of surface tractions $P_i$ is observed it too will possess a yield surface in a force space having a dimension equal to the number of the $P_i$. Denoting the plastic displacements corresponding to the $P_i$ as $u_i^P$ and superposing the axes of a plastic displacement space composed of the $u_i^P$ on the force space $P_i$, the attainment of yielding along some path in force space will again be accompanied by plastic flow. If the system is again comprised of a material exhibiting normality, the plastic displacement increment vector $d\vec{u}^{P}$ will also be parallel to the normal to the yield surface at the yield load $P_i^{Y}$. Conversely a system exhibiting normality in force space is comprised of materials exhibiting normality in stress space provided there is no frictional dissipation on the boundary of the system.

The failure envelope for sands is a surface definable in both force and stress space. A lack of normality to this surface in either space may be explained in two ways. Either the failure envelope is not a yield surface or the material itself does not exhibit normality. Discussion concerning the first of these concepts is given in Drucker et al (9), Jenike and Shield (18), Drucker (12) and Palmer (21) while the second is treated in Drucker (8), Palmer (21) and this author and Paslay (31). The purpose of this investigation was not to attempt resolution of this theoretical question, but simply to study

the character of the flow behavior of cohesionless soils at failure.

## EXPERIMENTAL PROCEDURE

This section contains a discussion of the experimental procedure followed in this investigation. A description of the testing device used and of any modifications to the generally accepted procedures for this device is included. Succeeding sections deal with the testing program, the results obtained, and the analysis of the data.

Conceptually the direct shear device provides a means for evaluating the effect of shearing stress on a prescribed plane of a soil as a function of the normal stress existing on that plane and the intrinsic properties of the material. In the late thirties and probably earlier, enough theoretical evidence had been presented to indicate that this simple conceptual picture of what the results of direct shear testing indicated, possessed only an accidental connection with reality. The state of stress and strain within a direct shear test specimen is exceedingly complex and any abstraction of the normal and tangential surface loads and their associated displacements for indicating pointwise material properties can not be substantiated. Soil researchers, on acceptance of these concepts, turned their efforts towards development of an apparatus theoretically capable of predicting point material properties in a finite sized specimen.

In this study only the forces and their associated displacements acting on the direct shear specimen are recorded. No attempt is made to abstract these results to the stress-strain level. The primary object of the study is to ascertain the relationship between the direction of the plastic deformation rate vector and the direction of the normal to the failure envelope. The inferences as to pointwise cohesionless soil properties from these results can only be qualitative. Nevertheless it should be kept in mind that the direct

shear test gives a serviceable indication of the magnitude of the friction angle, is reflective of initial void ratio, and, perhaps, most importantly predicts the flow in force-displacement terms of the stress-strain curves associated with triaxial testing. However, only further testing with triaxial equipment can substantiate the inferences made from the results presented herein.

Figs. 2, 3, and 4 show respectively for the device used in the investigation; a vertical cross section through the specimen in the plane of the applied tractions, an enlargement of this cross section, and a plan view of the apparatus. The various parts of importance in the ensuing discussion are indicated by capital letters and dimensions required for calculation by letters in lower case. The views shown in these three figures represent the disposition of the system prior to the application of the weight (A) and the horizontal thrust. The specific device used in the study was a Soiltest, Inc. Direct Shear Test Apparatus, Model D-110 equipped with a Soiltest, Inc. Direct Shear Box, Model D-183. The apparatus has been modified slightly to permit recording of the necessary data required in this investigation. A hand operated tangential thrust mechanism was selected, partially for better control over incrementing the tangential load, but primarily to eliminate the effect on vertical displacements of the vibrations of a previously used motorized apparatus.

Before discussing in detail the particular procedural aspects associated with this series of experiments, a brief description of a direct shear test is included to provide a base for the ensuing discussion. Reference will be made to the lettered parts of Figs. 2, 3, and 4. The sample (J) is placed at some initial density within the well formed by the upper ($H_1$) and lower ($H_2$) square shear box rings and the lower loading block ($D_2$). Parts ($H_2$) and ($D_2$) are rigidly attached to the shear box housing (F) and this combination may be

considered fixed with respect to ground. An assembly, which during the test may be considered rigid, consisting of the upper loading block ($D_2$), the yoke assembly (C) and the tilt bar (E) is then applied. In the normal test dial gages ($R_V$) and ($R_H$) are placed in the positions shown to record respectively the vertical movement of the tilt bar E and the horizontal displacement of the upper square shear box ring ($H_1$). After noting the initial readings of these dials, the vertical load is applied to the weight hanger (B) by weights (A) to a prescribed value. Subsequently, after pulling pins connecting the two shear box rings, a horizontal thrust is applied by a screw mechanism at the right of Fig. 2. The magnitude of this reactive thrust is determined using the dial gage ($R_P$) of the proving ring mounted in series with the feed screw. The thrust is transmitted from the proving ring to the reactor shaft and thence to the shear box coupling (G). The shear box coupling is rigidly attached to the upper square box ring ($H_1$). The reactive thrust drives this ring to the left and thus deforms the specimen, readings of the gages being taken at intervals. The upper loading block ($D_1$) remains fixed laterally with respect to the upper shear box ring ($H_1$) by means of the fins protruding from the loading block into the sample. During the loading process, however, the upper loading block ($D_1$) is free to translate vertically or to rotate.

The sample is said to have failed whenever the tangential thrust required to cause a increase in horizontal deformation begins to diminish. This conventional definition of failure in direct shear fits the concept of system instability found in Drucker (11) if the vertical and horizontal loads are the only tractions doing work on the sample, and the vertical load remains of constant magnitude. In the terminology of Drucker (11) a system is said to become unstable whenever the increment of work done on the system by the load increments $\Delta P_i$ acting thru their corresponding displacement increments $\Delta u_i$

becomes negative. Thus if readings are taken at intervals, instability of the system occurs in the interval between the $k^{th}$ and $k^{th}$ plus one readings if

$$\{P_i\ (k + 1) - P_i\ (k)\}\ \ \{u_i\ (k + 1) - u_i(k)\} < 0 \qquad (1)$$

i.e.

$$\{P_1\ (k + 1) - P_1\ (k)\}\ \ \{u_1\ (k + 1) - u_1\ (k)\}$$
$$+ \{P_2\ (k + 1) - P_2\ (k)\}\ \ \{u_2\ (k + 1) - u_2\ (k)\}$$
$$+ \ldots + \{P_n\ (k + 1) - P_n\ (k)\}\ \ \{u_n\ (k + 1) - u_n\ (k)\} < 0 \qquad (2)$$

for a system subjected to $n$ surface tractions doing work on the specimen.

For the specific device employed in this investigation the stresses in the sample tend to induce a rotation of the upper loading block ($D_2$) in a clockwise direction about an axis perpendicular to the plane of the diagram of Fig. 2. This rotation causes an appreciable moment on the upper surface of the specimen due the length of the yoke assembly (C). Evaluation of the magnitude of the rotation was determined by inclusion of the tilt bar (E) and the tilt gage ($R_T$) through a calculation to be mentioned in a subsequent paragraph. Although this was the only additional work producing force included in this investigation more subtle forms exist. For the present study, their effect on Inequality (2) and on the lack of normality was felt to be negligible. Two of these tractions which might be of consequence, however, are the possible shearing force set up in a vertical direction between the left hand interior wall of the upper shear box ring ($H_1$) and the specimen due to a relative displacement observed near failure between this wall and the specimen, and secondly a moment induced by rotation of the upper shear box ring ($H_1$) about an axis coincident with the intersection of the right hand exterior wall and lower surface of the ring ($H_1$). As the determination of the first of these force magnitude

is somewhat difficult and the estimations made of both their contributions being of small magnitude, the assessment of these two effects was not included in the testing program.

As indicated in the previous paragraphs three force variables will be considered to do work on the soil system: the horizontal or tangential traction $T$, the vertical normal load $N$, and a moment $M$ induced by rotation of the upper loading block. The three displacements corresponding to these forces are respectively: the horizontal displacement $\delta_T$ of the upper shear box ring ($H_1$), the vertical displacement $\delta_N$ of the midpoint of the lower surface of the upper loading block ($D_1$), and the rotation $\psi$ of this surface about an axis through its midpoint and normal to the plane of the tractions. Fig. 5 shows a unstressed soil specimen and the positive directions of these forces and their associated displacements. In Fig. 6 a schematic view of the initial and displaced configurations is presented. Using Fig. 3, 5 and 6 as references the following analytic expressions for the derived variables can be formulated. The initial tilt of the sample coincident with the lower edge of the loading block, designated as $\psi_o$ is

$$\psi_o = \sin^{-1} \{a_R - a_L)/h\} \tag{3}$$

where $h$ is the width of the shear box ring well in the plane of Fig. 3 and the dimensions $a_R$ and $a_L$ are averages of two depth gage readings taken from the top of the upper yoke assembly bar (C) to the points marked by the symbol ✱ on Fig. 4. Using these same depth gage readings and the initial tilt, the initial average specimen thickness, $t_o$, is determined from

$$t_o = d_1 - [\{d_3 - d_2\} - \{(a_L + a_R)/2\}]/\cos\psi_o) \tag{4}$$

In Eq. (4) the dimensions $d_1$, $d_3$, and $d_2$ are defined by Fig. 3. Knowledge of the specific gravity of the sand $G_s$, the sample weight $W_s$, the planer

area of the well $h^2$, the initial average specimen thickness, $t_o$, and the current vertical displacement $\delta_N$ enables a computation to be made of the initial and current average sample void ratio e, i.e.

$$e = \{G_s \gamma_w h^2 (t_o - \delta_N)/W_s\} - 1 \tag{5}$$

The vertical normal load N is the sum of the weights (A) designated by $N_a$ and the combined weight $N_o$ of the weight hanger (B), the yoke assembly (C), the tilt bar (E), and the upper loading block ($D_1$). Thus

$$N = N_o + N_a \tag{6}$$

Calculation of the remaining two force variables, T and M, and the three displacements $\delta_T$, $\delta_N$ and $\psi$ requires the use of the four dial gage readings $R_P$, $R_H$, $R_V$ and $R_T$. Positive readings of $R_P$ and $R_H$ were induced by shortening their respective stems while the reverse was true for $R_V$ and $R_T$. Denoting the difference between the current and initial readings of these four gages also by $R_P$, $R_H$, $R_V$ and $R_T$, the tangential thrust T is determined from

$$T = k_p \cdot R_P \tag{7}$$

$k_p$ being the proving ring constant. The horizontal displacement $\delta_T$ associated with the thrust T is simply equal to $R_H$. The current tilt angle $\psi_c$ (see Fig. 6) can be determined from

$$\psi_c = \tan^{-1}\{(a_T \cdot \sin\psi_o + R_T - R_V)/a_T \cos\psi_o\} \tag{8}$$

where $a_T$ is the initial distance along the tilt bar (E) between the centerlines of the dial gage stems $R_V$ and $R_T$. Hence the rotation $\psi$ becomes

$$\psi = \psi_c - \psi_o \tag{9}$$

The vertical displacement of the point Q of Fig. 6, denoted as $\delta_N$, and associated with the vertical normal force N can be shown to be

$$\delta_N = R_V + \delta_T \cdot \tan\psi_c + d_3\{(\cos\psi_c - \cos\psi_o) + \tan\psi_o (\sin\psi_c - \sin\psi_o)\} \tag{10}$$

Determination of the moment $M$ caused by the lateral displacement of the weights from a vertical line through point $Q$ is given by

$$M = \{N_o(r_c + d_2 - d_3) + N_a (r + d_2 - d_3)\} \cdot \sin\psi_c \quad (11)$$

with the dimension $r$ being defined by Figure 3 and $(r_c + d_2 - d_3)$ being the parallel distance from point $Q$ to the center of gravity of the combination of parts (B), (C), (E) and ($D_1$).

## TESTING PROGRAM

The particular sand selected for the series of experiments was a locally quarried quartz sand commonly used in the making of concrete. The material was screened and only particles passing a #20 mesh sieve (U.S. Standard) but retained on a #25 mesh sieve, were used in the testing program. Under the microscope, the grains appeared to have a predominantly angular shape. A determination of the specific gravity of the sand yielded a figure of 2.65 while additional tests indicated a possible void ratio range of 0.662-0.965 for the particles making up the samples.

In general the testing program involved preparing the specimen to some prescribed initial configuration, applying the normal load $N_a$ to a particular magnitude and finally applying the tangential thrust $T$ in increments, until the tangential displacement reached a value between 0.25 - 0.38 centimeters (0.10 - 0.15 inches). In some cases, however, this procedure was altered by cycling the tangential thrust, changing or cycling the normal load, or a combination of the above. Such nonstandard loading was included partially to ascertain its effect on failure but primarily to obtain information regarding the inelastic behavior of sands within the failure envelope. This latter subject will not be pursued in this report.

To characterize the individual tests, a group symbol has been assigned

to each, reflecting the initial configuration and the normal load N at failure. For example, 5zd indicates that the normal load at failure is of the 5th magnitude in a series of seven, the initial tilt z is in the zero range, and the initial average void ratio d is in the dense portion of the spectrum. Amplifying this terminology the seven final normal loads are: 1 - 7.8 kg, 2 - 11.8 kg, 3 - 19.8 kg, 4 - 35.8 kg, 5 - 51.8 kg, 6 - 67.8 kg and 7 - 83.8 kg. The initial tilt $\psi_o$ is indicated by the letter symbols p, z, and n. The letter p represents $+2.00^o \geq \psi_o \geq +0.68^o$, while z designates $+0.67^o \geq \psi_o \geq -0.67^o$ and n, $-0.68^o \geq \psi_o \geq -2.00^o$. Lastly, the initial average void ratio $e_o$ is characterized by the letters d, m, and l. A dense initial state, denoted by d, requires $0.662 \leq e_o \leq 0.761$, a medium initial state m, for $0.762 \leq e_o \leq 0.865$ and a loose initial state l, for $0.866 \leq e_o \leq 0.965$. Table I found in Appendix III depicts this grouping of the 107 test numbers making up the series of experiments.

In the performance of an actual test, readings of the dial gages were taken at each change of weight (A) and at each increment of tangential thrust. The gages were read in a systematic manner by a single operator and thirty seconds were allowed after each change of loading to permit the time effect, attendant to granular behavior, to subside. The size of each tangential thrust increment was in the neighborhood of 3 kg until the tangential displacement increment $\Delta_T$ reached a preset value. Control of the thrust mechanism was then shifted to the displacement gage, $R_H$. In this manner a well spaced set of values was obtained for plotting purposes and the work increments, defined by Inequality (2) were meaningful for locating the magnitude of the variables associated with failure. A computer was utilized in reducing the raw dial gage readings and other input to the variables defined by Inequality (2) and Eqs. (3) through (11).

Plots of various quantities for two typical tests are shown as Figs. 7, 8, 9 and 10. The two tests selected for plotting were Nos. 452 and 472 having group symbols 5zd and 5zl respectively. Fig. 7 shows projections of the three dimensional loading histories onto the T-N and T-M force planes while Fig.8 depicts projections the corresponding displacement histories. In Fig. 9 plots of the tangential thrust versus tangential displacement and normal load versus normal displacement are given. Finally Fig. 10 represents graphs of tangential thrust versus the configuration variables of relative sample density, RD, and the current tilt angle $\psi_c$ . The relative density is defined in the usual manner as

$$RD\ (\%) = \{(e_{max} - e)/\ (e_{max} - e_{min})\} \times 100 \qquad (12)$$

where $e_{max}$ and $e_{min}$ are respectively the void ratios corresponding the loosest and densest states (0.965 and 0.662).

As has been indicated in the preceding paragraphs and more succinctly by Table I, the testing program reported herein involved probing the soil system under investigation over a wide range of initial conditions and loading paths. A large number of tests was needed in order to provide sufficient data for determining a mathematical expression which would adequately represent the failure surface in a hyperspace of the three force variables and any necessary configuration parameters. The results of the experimental program are presented in the following section.

## TEST RESULTS

For the particular soil system discussed herein, failure of the specimen was assumed to have occurred in the interval between the $k^{th}$ and the $k^{th}$ plus one observations whenever Inequality (2) became satisfied. In terms of the work inducing forces acting on the system this Inequality may be rewritten as

$$\{T(k+1) - T(k)\}\cdot\{\delta_T(k+1) - \delta_T(k)\} + \{N(k+1) - N(k)\}\cdot\{\delta_N(k+1) - \delta_N(k)\}$$
$$+ \{M(k+1) - M(k)\}\cdot\{\psi(k+1) - \psi(k)\} \leq 0 \qquad (13)$$

Once this inequality is satisfied the actual forces selected as those acting at failure are the ones associated with the $k^{th}$ observation. Since the magnitudes of these forces change only slightly near failure for the interval sizes selected the maximum percent error between the real and selected force values at failure was estimated to be 2% with the average being somewhat less than 0.5%.

The values determined for the plastic displacement increments associated with failure were determined in the following manner and based on an assumption regarding the elastic displacements. Previous testing had indicated that on unloading from a force point near failure, the recoverable or elastic displacements were zero for a unloading increment corresponding in magnitude to the previous loading change. Thus the displacements occurring on loading from the $k^{th}$ to the $k^{th}$ plus one observation were totally irrecoverable or plastic. Stated in another way this assumption implies that the stiffness moduli associated with reversible behavior are three to four orders of magnitude larger than the moduli associated with irreversible behavior at failure and thus for displacement increments of 0.01" maximum, the elastic displacements would remain undetected in dial gage readings estimated to 0.00001". Based on this assumption the plastic displacement increments were simply the changes $\Delta\delta_T$, $\Delta\delta_N$, $\Delta\psi$ occurring in the interval in which Inequality (12) became satisfied. For the scale of Fig. 8 the displacement $\delta_N$ and the rotation $\psi$ appear to be fairly smooth functions of the displacement $\delta_T$ near failure but on a larger scale they are somewhat more ragged. Consequently the values of $\Delta\delta_N$ and $\Delta\psi$ actually reported represent unweighted smoothings of those portions of the $\delta_N - \delta_T$ and $\psi - \delta_T$ curves over five displacement increments centered on the increment in which Inequality (13) was initially satisfied.

Table II of Appendix III gives the configuration data of all the tests reported for both the initial and failure states. The test number indicates the chronological order of testing. In this sequence, the missing numbers are indicative of tests not carried to failure. The sand for each experiment came from the same source, was not reused, and all tests were performed by a single operator over a three month period. The laboratory temperature is kept at 21± 1$^{\circ}$ C with the relative humidity being 50± 10%. All samples were tested in the air dried condition. The forces and displacement increments at failure are listed in Table III of Appendix III. In the subsequent and final section of this paper the analysis made using the data of Tables II and III is presented and discussed.

## ANALYSIS OF TEST DATA

The analysis of the data contained in Tables II and III is essentially a two stage process. Initially a nest of failure envelopes in the force space of the applied tractions must be defined by an analytic expression from which normals may be determined. Subsequently a systematic comparison between the normals and the corresponding plastic displacement increment vectors must be made. In accomplishing this analysis process, various aspects of the statistical method are employed. These statistical techniques facilitate the handling of a large amount of data and more importantly are useful in helping to substantiate inferences made from the results.

In the first stage an analytic expression was sought which described failure of the system in terms of the force variables and the configuration parameters. The technique employed to determine this function was simply to fit a surface by the method of least squares, that would adequately predict the tangential thrust at failure in terms of the other variables. Pictorally such a function would yield a nest of failure envelopes in the force space of the

applied tractions. A single surface of the nest would be isolated by holding constant whatever configuration variables were necessary in defining the failure envelope function. As the sole purpose of this stage was to determine an analytic function from which normals could be extracted the question as to whether the form of the function eventually selected, was correct theoretically, appeared to be of secondary importance. Certain restrictions of a physical nature were, however, included in the development of the possible formulations. The selection of the failure tangential thrust as the dependent variable is, of course, somewhat arbitrary but considering the nature of the system tested, the choice was felt to be logical.

As previously mentioned, the independent variables were taken as the failure normal force and moment, and additionally those system configuration parameters necessary to formulate an adequate failure function. Such configuration parameters include the initial density, the initial tilt angle, and the magnitudes of the displacements and rotation at failure. How many of these parameters and what combinations of them would be required to formulate an adequate predictive equation for the tangential failure thrust were additional issues to be resolved in this first stage of the analysis.

The basic form of the expression chosen to predict the tangential thrust at failure was an infinite power series in the independent variables.

$$T_{fp} = \sum_{i=1}^{n} c_i^{(1)} X_i + \sum_{i=1}^{n} \sum_{j=1}^{n} c_{ij}^{(2)} X_i X_j + \ldots \qquad (14)$$

In Eq. (14) $T_{fp}$ is the predicted value of tangential thrust at failure, $X$ is the symbol for an independent variable and $c$ symbolizes the constants to be determined by the method of least squares. The actual independent variables required for an adequate predictive equation were eventually determined to be

the vertical normal force at failure $N_f$, the moment at failure $M_f$, and the failure void ratio $e_f$. In reality it can be seen from Eq. (11) that $M_f$ is a function of $N_f$ and the current tilt angle at failure $\psi_f$. Thus a somewhat more basic independent variable could be $\psi_f$, but since the requirements of the second stage of the analysis call for a normal vector with a component along the M axis, $M_f$ has been taken as independent. Some of the constants c can be set to zero in Eq. (14) if it is assumed that $T_f$ equals zero when $N_f$ is zero. This assumption was made in this analysis and thus all terms in the expanded version of Eq. (14) not containing $N_f$ as a variable are absent. The lowest powered form of Eq. (14) appearing to give satisfactory predictions for $T_f$ was the third. Rewriting Eq. (14) in expanded form up to the third power and incorporating the aforementioned physical assumption concerning $N_f$ yields

$$T_{fp} = b_1N_f + b_2N_f^2 + b_3N_fM_f + b_4N_fe_f + b_5N_f^3 + b_6N_f^2M_f + b_7N_f^2e_f + b_8N_fM_f^2 + b_9N_fM_fe_f + b_{10}N_fe_f^2 \qquad (15)$$

where the $b_i$ represent the constants to be determined from the method of least squares. On performing the numerical analysis the actual equation obtained from the input of Tables II and III is

$$T_{fp} = -0.17749947\ N_f - 0.01211425\ N_f^2 + 0.00783852\ N_fM_f + 5.20248222\ N_fe_f + 0.00002449\ N_f^3 - 0.00001539\ N_f^2M_f + 0.00985996\ N_f^2e_f - 0.00002242\ N_fM_f^2 - 0.00571806\ N_fM_fe_f - 4.62136745\ N_fe_f^2 \qquad (16)$$

The standard error of estimate of $T_f$ on $N_f$, $M_f$ and $e_f$, symbolized by $s_{T_f.N_fM_fe_f}$ is a measure of the scatter about the regression surface of $T_f$ on $N_f$, $M_f$ and $e_f$. Surfaces parallel to that of Eq. (16) $\pm s_{T_f.N_fM_fe_f}$ kg from

it along the T axis should contain 68% of all the sample points if the randomness is normally distributed. $s_{T_f \cdot N_f M_f e_f}$ is defined as

$$s_{T_f \cdot N_f M_f e_f} = \left[ \frac{\sum_{i=1}^{n} (T_{fi} - T_{fpi})^2}{n} \right]^{\frac{1}{2}} \tag{17}$$

In Eq. (17) n is the number of tests, the other symbols being previously defined. For the data of this series $s_{T_f \cdot N_f M_f e_f}$ was found to be 1.8003 kg. A somewhat more unbiased estimate of the standard error of estimate replaces the denominator of Eq. (16) by the number of degrees of freedom. As ten constants exist in Eq. (15) and nine more were set to zero by the physical assumption, the number of degrees of freedom is (n-19). Hence the unbiased standard error of estimate is 1.9851 kg.

The square root of the quotient obtained by dividing the explained variation of $T_f$ by the total variation of $T_f$ is known as the coefficient of multiple correlation, $R_{T_f \cdot N_f M_f e_f}$. In this expression the total variation is simply the variance or square of the standard deviation of $T_f$ while explained variation is the variance of $T_f$ minus the square of $s_{T_f \cdot N_f M_f e_f}$. Allowing $s_{T_f}^{\ 2}$ to stand for the variance of $T_f$ the coefficient of multiple correlation may be expressed symbolically as

$$R_{T_f \cdot N_f M_f e_f} = \left[ 1 - \frac{s_{T_f \cdot N_f M_f e_f}^{\ 2}}{s_{T_f}^{\ 2}} \right]^{\frac{1}{2}} \tag{18}$$

Performing the required calculation yielded $R_{T_f \cdot N_f M_f e_f}$ equal to 0.9952. As a perfect correlation between the actual failure thrusts and those predicted by Eq. (16) would be unity, it was felt that Eq. (16) adequately represented the function describing the nest of failure envelopes.

The dashed lines of Figs. 11 through 16 show intersections of failure surfaces as determined by Eq. (16) with various planes, $M$ equal a constant or $N$ equal a constant, for four values of relative density (0%, 33%, 67% and 100%). Also, as the various titles of the figures indicate, the information contained in Tables II and III is pictorally displayed. Cursory examination of the figures indicates the nature of the agreement between Eq. (16) and the actual tangential thrusts at failure. Projections of the plastic displacement increment vectors onto planes where $N$ is constant seem to be normal to the failure envelope while projections of these same vectors onto planes $M$ equal a constant clearly evidence a lack of normality.

The second stage of the analysis was directed towards systematically studying the relationship between the direction of the observed plastic deformation increment vector and that of the analytically determined normal to the failure envelope. For a given test the directional cosines of the normal in the force space of the applied tractions were obtained by differentiating Eq. (16) with respect to $N_f$ and $M_f$. The partial derivatives $\partial T_{fp}/\partial N_f$ and $\partial T_{fp}/\partial M_f$ thus obtained represent slopes of the projections of the normal vector onto the planes $M = 0$ and $N = 0$ respectively. Inserting the particular values of $N_f$, $M_f$, and $e_f$ associated with the test in question into the analytical expressions for $\partial T_{fp}/\partial N_f$ and $\partial T_{fp}/\partial M_f$ yielded numerical values for the slopes of the projections from which the directional cosines of the normal vector could be calculated. As Eq. (16) represents a parametric nest of surfaces in force space best fitting the data, there exists the somewhat obvious observation that the directional cosines calculated by the procedure described above would be somewhat different from those obtained by entering Eq. (16) with the observed values $T_f$, $N_f$ and $M_f$. This latter method would yield a value of failure void ratio different from the observed

$e_f$ and thus, eventually, modified values for the directional cosines of the normal. Actually from a statistical standpoint a more elaborate procedure would be necessary to obtain a less biased set of values for the directional cosines of the normals. Such a procedure would involve formulation of four equations of the type exemplified by Eq. (14) with each expression having a different dependent variable. Relaxation of the bias introduced by the physical assumption which set certain constants to zero would also be necessary. Manipulation of each resulting equation would collectively yield four sets of values for the directional cosines of any particular normal that could then be averaged. Although this last mentioned method is theoretically more sound, the close correlation of Eq. (16) to the observed data as expressed by the value of $R_{T_f \cdot N_f M_f e_f}$ strongly suggests that the simplified technique used herein to determine the direction of the normals is adequate.

Having the directional cosines of both the normal and flow increment vectors at failure for each test, the specific purpose of this investigation could now be undertaken. For the purpose of clarity a set of unit vectors $\vec{i}$, $\vec{j}$ and $\vec{k}$ are taken to act respectively along the M, N, and T axes of the force space. Denoting the directional cosines of the normal to the failure envelope to the M, N and T axes by $\ell_n$, $m_n$ and $n_n$ respectively, and the directional cosines of the displacement increment vector to these same axes by $\ell_d$, $m_d$ and $n_d$ the following unit vectors may be defined for each test result as

Plastic Displacement Increment Vector $= \Delta\vec{\delta} = \ell_d\vec{i} + m_d\vec{j} + n_d\vec{k}$ (19.a)

Normal Vector $= \vec{\nu} = \ell_n\vec{i} + m_n\vec{j} + n_n\vec{k}$ (19.b)

Further define the projections of these vectors onto the planes M equal zero and N equal zero by the superscripts NT and MT respectively, i.e.

$$\Delta\vec{\delta}^{NT} = m_d\vec{j} + n_d\vec{k} \tag{20.a}$$

$$\Delta\vec{\delta}^{MT} = \ell_d\vec{i} + n_d\vec{k} \tag{20.b}$$

$$\vec{\nu}^{NT} = m_n\vec{j} + n_n\vec{k} \tag{20.c}$$

$$\vec{\nu}^{MT} = \ell_n\vec{i} + n_n\vec{k} \tag{20.d}$$

A systematic study of the relationship between $\Delta\vec{\delta}$ and $\vec{\nu}$ for each test is facilitated by calculation of the following angles.

$$\theta_A = \cos^{-1}[(\vec{\nu}\cdot\vec{k})/(|\vec{\nu}||\vec{k}|)] \tag{21.a}$$

$$\theta_B = \cos^{-1}[(\Delta\vec{\delta}\cdot\vec{k})/(|\Delta\vec{\delta}||\vec{k}|)] \tag{21.b}$$

$$\theta_C = \cos^{-1}[(\vec{\nu}\cdot\Delta\vec{\delta})/(|\vec{\nu}||\Delta\vec{\delta}|)] \tag{21.c}$$

$$\theta_D = \cos^{-1}[(\vec{\nu}^{MT}\cdot\vec{k})/(|\vec{\nu}^{MT}||\vec{k}|)] \tag{21.d}$$

$$\theta_E = \cos^{-1}[(\Delta\vec{\delta}^{MT}\cdot\vec{k})/(|\vec{\Delta\delta}^{MT}||\vec{k}|)] \tag{21.e}$$

$$\theta_F = \cos^{-1}[(\vec{\nu}^{MT}\cdot\Delta\vec{\delta}^{MT})/(|\vec{\nu}^{MT}||\vec{\Delta\delta}^{MT}|)] \tag{21.f}$$

$$\theta_G = \cos^{-1}[(\vec{\nu}^{NT}\cdot\vec{k})/(|\vec{\nu}^{NT}||\vec{k}|)] \tag{21.g}$$

$$\theta_H = \cos^{-1}[(\Delta\vec{\delta}^{NT}\cdot\vec{k})/(|\Delta\vec{\delta}^{NT}||\vec{k}|)] \tag{21.h}$$

$$\theta_I = \cos^{-1}[(\vec{\nu}^{NT}\cdot\Delta\vec{\delta}^{NT})/(|\vec{\nu}^{NT}||\Delta\vec{\delta}^{NT}|)] \tag{21.i}$$

Fig. 17 illustrates the vectors and angles defined by Eqs. (19) through (21). Since the angles given by Eqs. (21.d) through (21.i) are restricted to lie in the planes M equal zero or N equal zero they can be assigned positive or negative values. The convention adopted is based on the following equalities:

$$\theta_D > 0 \text{ if } (\ell_n/n_n) > 0 \tag{22.a}$$

$$\theta_E > 0 \text{ if } (\ell_d/n_d) > 0 \tag{22.b}$$

$$\theta_F > 0 \text{ if } [(\ell_d/n_d) - (\ell_n/n_n)] > 0 \tag{22.c}$$

$$\theta_G > 0 \text{ if } (m_n/n_n) > 0 \tag{22.d}$$

$$\theta_H > 0 \text{ if } (m_d/n_d) > 0 \tag{22.e}$$

$$\theta_I > 0 \text{ if } [(m_d/n_d) - (m_n/n_n)] > 0 \tag{22.f}$$

Ordering of angles $\theta_A$, $\theta_B$, and $\theta_C$ was not attempted partially because such a process is somewhat involved but primarily because sufficient information was obtained by simply considering their absolute magnitudes. Calculation of angles $\theta_D$ and $\theta_G$ is somewhat redundant but the listing of these values enables a faster visualization of the behavior of the normal vector.

Having thus defined the angular relationships expressed by Eqs. (21), the initial part of this second phase of analysis was simply to compute the numerical values of these quantities for each of the tests reported. Once such a listing is determined an obvious beginning to studying the character of the flow is simply to compute the means and standard deviations of each of the angular measures. The results of this computation are given in Table IV of Appendix III. One result appears to stand out immediately. The mean of the angles $\theta_F$ denoted as $\tilde{\theta}_F$, is very close to zero. Reference to Fig. 17 or Eq. (21.f) discloses that such a value for $\tilde{\theta}_F$ indicates that normality or something quite close to it exists as an average in planes where N equals a constant. A second result of somewhat obvious nature is that normality does not exist in the planes of constant M . This is shown by the value of $\tilde{\theta}_I$, which has a magnitude of $-26.72^\circ$. The value of $\tilde{\theta}_C$ of $26.76^\circ$ reflects both the magnitudes of $\tilde{\theta}_I$ and $\tilde{\theta}_F$ . Geometrically $\tilde{\theta}_C$ represents the average co-latitude of the flow vector from a normal vector coincident with a polar axis. The importance of the near normality result indicated by $\tilde{\theta}_F$ is essentially to place all of the variance from normality indicated by the magnitude of $\tilde{\theta}_C$ into planes of constant M . For the system studied in this investigation, then, lack of normality can be studied by simply concentrating on the projections of the normal and flow vectors onto the plane of zero

moment. Before this can be done, however, one final check should be made on the distribution of $\tilde{\theta}_F$. This check involves determining if the various values of $\theta_F$ about $\tilde{\theta}_F$ vary randomly, or whether functional relationships exist between the $\theta_F$ and the various force or system parameters existing at failure. Two parameters, $\psi_f$ and $RD_f$, were selected for this check. The results of these plots are shown as Figs. 18 and 19. The first of these figures depicts a plot of the various $\theta_F$ versus their corresponding $RD_f$ and indicates no functional relationship existing. The second figure, however, does appear to show some slight dependence of the $\theta_F$ on $\psi_f$. This dependence indicates that the divergence from normality in planes of constant N may increase with increasing positiveness of $\psi_f$ at failure. Accompanying this trend and making it somewhat more difficult to interpret is a decided increase in the deviations about the mean at both ends of the investigated $\psi_f$ spectrum. As Fig. 19 does not appear to conclusively demonstrate dependence of $\theta_F$ on $\psi_f$ it will be assumed that near normality with random variance exists in planes of constant normal force.

The character of the definite lack of normality in planes of constant moment as indicated by the magnitude of $\tilde{\theta}_I$ may also be investigated by the techniques of the previous paragraph. As previous effort in this area both in triaxial and direct shear testing has given rise to the phrase "constant volume flow," a phrase which implies that the rate of volume change at failure is zero for certain relative densities, it is of interest to also study the behavior of the angle between the projection of the displacement increment vector onto the M equal zero plane and the T axis, i.e. $\theta_H$. The obvious parameter of importance here is the final relative density and plots of $\theta_I$ and $\theta_H$ versus this parameter are shown in Fig. 20. As is evident from the graph both $\theta_I$ and $\theta_H$ at failure are dependent on the relative

density. Assuming a linear trend for both plots the following regression lines were determined.

$$\theta_H = 2.28 - 0.2582\ RD_f \tag{23.a}$$

$$\theta_I = -33.36 + 0.1184\ RD_f \tag{23.b}$$

These had correlation coefficients as determined by an appropriately modified form of Eq. (18) of 0.905 and 0.792 respectively. The ninety-five % confidence limits on the slope of Eqs. (23.a) and (23.b) were ±0.0817 and ±0.1179. A closer look at Figure 20 indicates that a parabolic curve might be a better trend for $\theta_H$ versus $RD_f$ but that little would be gained by use of such a form for $\theta_I$ versus $RD_f$. Calculations were not, however, carried out to substantiate these observations.

## DISCUSSION AND SUMMARY

For the system investigated normality to the failure surface appears to exist for projections of the flow increment vector onto planes of constant normal load. This is indicated by the nearly zero mean value of $\theta_F$ and the absence of any conclusive functional dependence on the various force and configuration failure parameters. On projecting the flow increment vector onto planes of constant moment a decided lack of normality is seen. As a first approximation the magnitude of the angular deviation may be regarded as a constant with a mean value of $-26.72^\circ$ and a standard deviation of $\pm 3.21^\circ$. Closer examination reveals, however, that a functional relationship exists between $\theta_I$ and $RD_f$. This can be seen in Fig. 20 or determined from Eq. (23.b). The slope term in Eq. (23.b) indicates that the probable angular deviation from normality has a range of values confined to a fan having a central angle of $11.32^\circ$. Most natural sands have relative densities within the extremes of 0 and 100% and thus the plausibility of using a con-

stant value (say - $27.44^{\circ}$ at $RD_f$ = 50%) to describe the deviation from normality is not unrealistic.

Before attempting to draw any inferences from these results regarding the possible pointwise behavior of a cohesionless soil, two important limitations of the testing program described in this paper should be discussed. The first of these is that the final loading path to failure in all tests was confined to planes of constant normal load. Consequently, whether or not the various results are path independent has not been shown. The second limitation is simply that since only one specific sand was tested in a single device there can be no assurance that the results can be applied to a wide spectrum of granular media. Beside these limitations it perhaps should be repeated that inferences drawn from observations on a system can only be qualitative in their applicability towards the formulation of stress-strain relations.

The development of these inferences may be made clearer by reference to Fig. 21. The principal stress space $\sigma_1$, $\sigma_2$, $\sigma_3$ shown in Fig. 21.a assumes compressive stresses to be positive. Hydrostatic pressures are located on the space diagonal where $\sigma_1 = \sigma_2 = \sigma_3$ . On superposing the axes of a principal plastic strain space $\varepsilon_1^p$, $\varepsilon_2^p$, $\varepsilon_3^p$ on their counterparts in principal stress space, plastic volume increases have the same direction as that of the negative space diagonal. The $\pi$-plane in Fig. 21.a is perpendicular to the space diagonal. A stress or plastic strain increment vector lying in the $\pi$ plane has no hydrostatic or dilatation rate component. The simplest analytical representations of the failure surface in principal stress space for cohesionless soils are cones or pyramids with hexagonal bases. The apexes of these surfaces are located at the origin of coordinates and they open outward with increasing hydrostatic pressure maintaining a minimum of three-fold

symmetry about the space diagonal. The rate at which these surfaces diverge from the space diagonal is a function of the current relative density of the material. Intersections of three of these surfaces with the $\pi$-plane for a specific relative density are shown in Fig. 21.b.

The implications of the results of this become clearer if the normal force axis (N) of the force space of applied tractions acting on the direct shear specimen is superposed on the hydrostatic axis of the principal stress space. That this can be done is based on the fact that the system volume change is reflected only in the displacement $\delta_N$ . The first implication is that since normality is preserved in planes of constant normal force it is preserved in the $\pi$-plane of principal stress space. The second implication is that the lack of normality in planes perpendicular to the $\pi$-plane may be of approximately constant angular magnitude.

## APPENDIX I. - REFERENCES


1. Barden, L. and Khayatt, A. J., "Incremental Strain Rate Ratios and the Strength of Sand in the Triaxial Test," Geotechnique, Vol. 16, No. 4, Dec., 1966, pp. 338-357.

2. Bishop, A. W. and Green, G. E., "The Influence of End Restraint on the Compression Strength of a Cohesionless Soil," Geotechnique, Vol. 15, No. 3, Sept., 1965, pp. 243-266.

3. Broms, B. B. and Jamal, A. K., "Analysis of the Triaxial Test, Cohesionless Soils," Proceedings, Sixth International Conference on Soil Mechanics and Foundation Engineering, Montreal, Vol. I, pp. 184-188.

4. Brown, E. H., "A Theory for the Mechanical Behavior of Sand," Proceedings, Eleventh International Congress of Applied Mechanics, Munich, 1964, Springer Verlag, Berlin-Heidelberg-New York, 1966, pp. 183-191.

5. Cornforth, D. H., "Some Experiments on the Influence of Strain Conditions on the Strength of Sand," Geotechnique, Vol. 14, No. 2, June, 1964, pp. 143-167.

6. Drucker, D. C., and Prager, W., "Soil Mechanics and Plastic Analysis or Limit Design," Quarterly of Applied Math., Vol. 10, No. 2, 1952, pp. 157-165.

7. Drucker, D. C., "Limit Analysis of Two and Three Dimensional Soil Mechanics Problems," Journal of the Mechanics and Physics of Solids, Vol. 1, 1953, pp. 217-226.

8. Drucker, D. C., "Coulomb Friction, Plasticity, and Limit Loads," Journal of Applied Mechanics, Vol. 21, 1954, pp. 71-74.

9. Drucker, D. C., Gibson, R. E., and Henkel, D. J., "Soil Mechanics and Work-Hardening Theories of Plasticity," Transactions, ASCE, Vol. 122, Paper No. 2864, 1957, pp. 338-346.

10. Drucker, D. C., "On Stress-Strain Relations for Soils and Load Carrying Capacity," Proceedings, First International Conference on Soil-Vehicle Systems, Turin, Italy, Edizioni Minerva Tecnica, June, 1961, pp. 15-23.

11. Drucker, D. C., "On the Postulate of Stability of Material in the Mechanics of Continua, Journal de Mecanique, Vol. 3, 1964, pp. 235-249.

12. Drucker, D. C., "Concept of Path Independence and Material Stability for Soils," IUTAM Symposium, Rheology and Soil Mechanics, J. Kravtchenko and P. M. Sirieys, eds.,Grenoble, France, April, 1964, Springer Verlag, Berlin-Heidelberg-New York, 1966, pp. 23-46.

13. Hansen, J. Brinch, Earth Pressure Calculation, Danish Technical Press, Copenhagen, Denmark, 1953.

14. Haythornthwaite, R. M., "Stress and Strain in Soils," Plasticity, Proceedings of the Second Symposium on Naval Structural Mechanics, E. H. Lee and P. S. Symonds, eds., Providence, R. I., April, 1960, Pergamon Press, London, 1960, pp. 185-193.

15. Haythornthwaite, R. M., Mechanics of the Triaxial Test for Soils, Journal of the Soil Mechanics and Foundations Division, ASCE, Vol. 86, No. SM5, Proc. Paper 2625, Oct., 1960, pp. 35-61.

16. Haythornthwaite, R. M., Discussion of Wu, T. H. et al., Reference 33, Journal of the Soil Mechanics and Foundations Division, ASCE, Vol. 89 No. SM5, Sept., 1963, pp. 119-120.

17. Horne, M. R., "The Behavior of an Assembly of Rotund, Rigid, Cohesionless Particles, Parts I and II," Proceedings of the Royal Society, Series A, Vol. 286, 1964, pp. 62-97.

18. Jenike, A. W., and Shield, R. T., "On the Plastic Flow of Coulomb Solids Beyond Original Failure," Journal of Applied Mechanics, Vol. 26, Dec., 1959, pp. 599-602.

19. Kirkpatrick, W. M., "The Condition of Failure for Sands," Proceedings, Fourth International Conference on Soil Mechanics and Foundation Engineering, London, Vol. I, 1957, pp. 172-178.

20. Ko, H. Y., and Scott, R. F., "A New Soil Testing Apparatus" Geotechnique, Vol. 17, No. 1, March, 1967, pp. 40-57.

21. Palmer, A. C., "On Stress-Strain Relations for Soils," Division of Engineering Report, NSF-GP 1115/19, Brown University, March, 1965, 87 pp.

22. Prager, W., "The General Theory of Limit Design," Proceedings, Eighth International Conference of Applied Mechanics, Istanbul, Vol. II, 1952, pp. 65-72.

23. Roscoe, K. H., Schofield, A. N., and Wroth, C. P., "On the Yielding of Soils," Geotechnique, Vol. 8, 1958, pp. 22-53.

24. Roscoe, K. H., Schofield, A. N., and Thurairajah, A., "An Evaluation of Test Data for Selecting a Yield Criterion for Soils," Laboratory Shear Testing of Soils, ASTM, Special Technical Publication 361, 1964, pp. 111-128.

25. Rowe, P. W., "The Stress-Dilatancy Relation for the Equilibrium of an Assembly of Particles in Contact," Proceedings of the Royal Society, Series A, Vol. 269, 1962, pp. 500-527.

26. Rowe, P. W., "Stress-Dilatancy, Earth Pressure, and Slopes," Journal of the Soil Mechanics and Foundations Division, ASCE, Vol. 39, No. SM3, Proc. Paper 3507, May, 1963, pp. 37-61.

27. Rowe, P. W. and Barden, L., "Importance of Free Ends in Triaxial Testing," Journal of the Soil Mechanics and Foundations Division, ASCE, Vol. 90, No. SM1, Proc. Paper 3753, Jan., 1964, pp. 1-27.

28. Shield, R. T., "Mixed Boundary Value Problems in Soil Mechanics," Quarterly of Applied Math., Vol. 11, No. 1, 1953, pp. 61-75.

29. Shield, R. T., "Stress and Velocity Fields in Soil Mechanics," Journal of Mathematical Physics, Vol. 33, 1954, pp. 144-156.

30. Shield, R. T., "On Coulomb's Law of Failure in Solids," Journal of the Mechanics and Physics of Solids, Vol. 4, 1955, pp. 10-16.

31. Weidler, J. B. and Paslay, P. R., "An Analytical Description of the Behavior of Granular Media," Division of Engineering Report, ARPA SD-86, No. E36, Brown University, Nov., 1966, 32 pp.

32. Williams, E. J., Regression Analysis, John Wiley and Sons, Inc., New York, 1959.

33. Wu, T. H., Loh, A. K., and Malvern, L. E., "Study of Failure Envelope of Soils," Journal of the Soil Mechanics and Foundations Division, ASCE, Vol. 89, No. SM1, Proc. Paper 3430, Feb. 1963, pp. 145-181.

## APPENDIX II. - NOTATION

$A$ = weights applied to produce normal load (see Fig. 2);

$a_L$ = average of left side depth gage readings (see Figs. 3, 4, and 6);

$a_R$ = average of right side depth gage readings (see Figs. 3, 4, and 6);

$a_T$ = distance along tilt bar from the intersections of the centerlines of the vertical and tilt dial gages with top surface of tilt bar (see Fig. 3);

$B$ = weight hanger, direct shear device (see Fig. 2);

$b_i$ = symbol for constants to be determined by method of least squares ($i$ = i, 2, 3 ...);

$C$ = yoke assembly, direct shear device (see Figs. 2, 3, and 5);

$c$ = general symbol for constants in Taylor series;

$D_1$ = upper loading block, direct shear device (see Figs. 2, 3, and 5);

$D_2$ = lower loading block, direct shear device (see Figs. 2 and 3);

$d$ = grouping symbol for specimens having an initial relative density between 66.7% and 100.0%.

$d\vec{u}^p$ = generalized plastic displacement increment vector;

$d\vec{\varepsilon}^p$ = plastic strain increment vector (see Fig. 1);

$d_1$ = depth dimension from top surface of upper shear box ring ($H_1$) to upper surface of lower loading block ($D_2$) (see Fig. 3);

$d_2$ = measured thickness of tilt bar (E) (see Fig. 3);

$d_3$ = combined measured thickness of top bar of yoke assembly (C), upper loading block ($D_1$) and tilt bar (E) (see Fig. 3);

$E$ = tilt bar, direct shear device (see Figs. 2, 3, and 4);

$e$ = average void ratio of specimen;

$e_o$ = initial average void ratio of specimen;

$e_f$ = void ratio of specimen at failure;

$e_{max}$ = loosest void ratio obtainable for sand used in experiments = 0.965;

$e_{min}$ = densest void ratio obtainable for sand used in experiments = 0.662;

$F$ = shear box housing, direct shear device (see Figs. 2, 3, and 4);

$f(\ )$ = function of;

$G$ = shear box coupling, direct shear device (see Figs. 2 and 3);

$G_s$ = specific gravity of sand used in experiments = 2.65;

$H_1$ = upper shear box ring, direct shear device (see Figs. 2, 3, and 4);

$H_2$ = lower shear box ring, direct shear device (see Figs. 2 and 3);

$h$ = interior horizontal dimension of square shear box ring (see Figs. 2 and 5);

$i$ = subscript ($i$ = 1, 2, 3 ...);

$\vec{i}$ = unit vector along moment axis of general force space;

$J$ = specimen, direct shear device (see Figs. 2 and 3);

$j$ = subscript ($j = 1, 2, 3 \ldots$);

$\vec{j}$ = unit vector along normal load axis of general force space;

$K$ = right hand side of yield function equation (see Fig. 1);

$k$ = index subscript denoting $k^{th}$ observation of dial gages during test;

$\vec{k}$ = unit vector along tangential force axis of general force space;

$k_p$ = proving ring constant;

$l$ = grouping symbol for specimens having an initial relative density between 0.0% and 33.3%;

$\ell_d$ = direction cosine between displacement increment vector at failure and moment axis;

$\ell_n$ = direction cosine between the normal vector to the failure envelope and the moment axis;

$M$ = moment acting on specimen induced by rotation of specimen upper surface (see Fig. 5);

$M_f$ = moment acting on specimen at failure;

$m$ = grouping symbol for specimens having an initial relative density between 33.3% and 66.7%;

$m_d$ = direction cosine between displacement increment vector at failure and normal load axis;

$m_n$ = direction cosine between the normal vector to the failure envelope and the normal load axis;

$N$ = normal or vertical load acting on specimen (see Fig. 5);

$N_a$ = that portion of the normal load on the specimen due to the weights (A);

$N_f$ = normal load acting on specimen at failure;

$N_o$ = that portion of the normal load on the specimen; due to the combined weights of the direct shear device parts (B), (C), ($D_1$) and (E);

$n$ = grouping symbol for specimens having an initial upper surface tilt angle between $-0.68^\circ$ and $-2.00^\circ$;

$n_d$ = direction cosine between displacement increment vector at failure and the tangential force axis;

$n_n$ = direction cosine between the normal vector to the failure envelope and the tangential force axis;

$P_i$ = generalized force variable;

$P_i^Y$ = yield load in force space;

$p$ = grouping symbol for specimens having an initial upper surface tilt angle between $+0.68^\circ$ and $+2.00^\circ$;

$R_H$ = symbol for tangential displacement dial gage and the reading of this gage (see Figs. 2 and 3);

$R_P$ = symbol for proving ring dial gage and the reading of this gage (see Figs. 2 and 4);

$R_T$ = symbol for tilt dial gage and the reading of this gage (see Figs. 2 and 3);

$R_{T_f \cdot N_f M_f e_f}$ = coefficient of multiple correlation of the tangential force at failure on the normal force, moment and void ratio at failure;

$R_V$ = symbol for vertical displacement dial gage and the reading of this gage (see Figs. 2 and 3);

$RD$ = average relative density of specimen;

$RD_f$ = average relative density of specimen at failure;

$RD_o$ = initial average relative density of specimen;

$r$ = distance along centerlines of yoke assembly bars (C) from lower surface of tilt bar (E) to contact point of parts (B) and (C);

$r_c$ = distance along centerlines of yoke assembly bars (C) from lower surface of tilt bar (E) to center of gravity of parts (B), (C), (D) and (E);

$s_{T_f}$ = standard deviation of the variable $T_f$;

$s_{T_f \cdot N_f M_f e_f}$ = standard error of estimate of the tangential force at failure on the normal load, moment and void ratio at failure;

$T$ = tangential or horizontal force acting on specimen (see Fig. 5);

$T_f$ = tangential force on specimen at failure;

$T_{fp}$ = tangential force at failure predicted by regression equation;

$u_i$ = generalized displacement;

$u_i^p$ = generalized plastic displacement;

$W_s$ = weight of specimen;

$X$ = independent variable in a regression analysis;

$Y$ = dependent variable in a regression analysis;

$z$ = grouping symbol for specimens having an initial upper surface tilt angle between $+0.67^\circ$ and $-0.67^\circ$;

$\gamma_w$ = unit weight of water;

$\Delta\delta_N$ = displacement increment in direction of normal force at failure;

$\Delta\delta_T$ = displacement increment in direction of tangential force at failure;

$\Delta\vec{\delta}$ = unit plastic displacement increment vector at failure (see Fig. 17);

$\Delta\vec{\delta}^{MT}$ = projection of unit plastic displacement increment vector at failure on plane N = 0;

$\Delta\vec{\delta}^{NT}$ = projection of unit plastic displacement increment vector at failure on plane M = 0;

$\Delta\psi$ = rotation increment in direction of moment at failure;

$\delta_N$ = displacement in direction of normal force N (see Fig. 5);

$\delta_T$ = displacement in direction of tangential force T (see Fig. 5);

$\varepsilon_1^p$, $\varepsilon_2^p$, $\varepsilon_3^p$ = principal plastic strains;

$\theta_A$ = angle between normal vector $\vec{\nu}$ and T axis (see Fig. 17);

$\theta_B$ = angle between displacement increment vector $\Delta\vec{\delta}$ and T axis (see Fig. 17);

$\theta_C$ = angle between $\vec{\nu}$ and $\Delta\vec{\delta}$ (see Fig. 17);

$\theta_D$ = angle between $\vec{\nu}^{MT}$ and T axis (see Fig. 17);

$\theta_E$ = angle between $\Delta\vec{\delta}^{MT}$ and T axis (see Fig. 17);

$\theta_F$ = angle between $\vec{\nu}^{MT}$ and $\Delta\vec{\delta}^{MT}$ (see Fig. 17);

$\theta_G$ = angle between $\vec{\nu}^{NT}$ and T axis (see Fig. 17);

| | | |
|---|---|---|
| $\theta_H$ | = | angle between $\Delta\vec{\delta}^{NT}$ and T axis (see Fig. 17); |
| $\theta_I$ | = | angle between $\vec{\nu}^{NT}$ and $\Delta\vec{\delta}^{NT}$ (see Fig. 17); |
| $\vec{\nu}$ | = | unit normal vector to the failure envelope (see Fig. 17); |
| $\vec{\nu}^{MT}$ | = | projection of $\vec{\nu}$ onto plane N = 0; |
| $\vec{\nu}^{NT}$ | = | projection of $\vec{\nu}$ onto plane M = 0; |
| $\sigma_{ij}$ | = | general state of stress; |
| $\sigma_{ij}^{Y}$ | = | general state of stress causing yield; |
| $\sigma_1$, $\sigma_2$, $\sigma_3$ | = | principal stresses; |
| $\phi_{df}$ | = | angle of internal friction at failure as determined in direct shear test; |
| $\phi_{dcvf}$ | = | angle of internal friction at failure in a direct shear test showing flow at constant volume; |
| $\psi$ | = | rotation in direction of moment M (see Fig. 5); |
| $\psi_c$ | = | current angular deflection of specimen upper surface from horizontal or current angle of tilt (see Fig. 6); |
| $\psi_o$ | = | initial angular deflection of specimen upper surface from horizontal or initial angle of tilt (see Figs. 5 and 6); |
| $\psi_f$ | = | angle of tilt at failure. |

APPENDIX III. - TABLE I

GROUPING OF TESTS BASED ON NORMAL LOAD AT FAILURE AND INITIAL CONFIGURATION

| Final Normal Load N (kg.) | Initial Tilt Angle $\psi_o$ | Initial Void Ratio | | | | | |
|---|---|---|---|---|---|---|---|
| | | Group Symbol | Loose | Group Symbol | Medium | Group Symbol | Dense |
| 7.8 | Zero | | | | | 1zd | 462 |
| 11.8 | Zero | | | 2zm | 482 | 2zd | 463 |
| 19.8 | Pos. | 3pl | 513 | 3pm | 464, 474, 525 | 3pd | 442, 458, 501 |
| | Zero | 3zl | 468, 470 512 | 3zm | 483, 517 | 3zd | 401, 450, 500 |
| | Neg. | 3nl | 511 | 3nm | 478, 499, 521 | 3nd | 499, 454 |
| 35.8 | Pos. | 4pl | 510 | 4pm | 465, 475, 524 | 4pd | 443, 459, 498 |
| | Zero | 4zl | 431 433*, 469, 471 509 | 4zm | 421* 484, 497, 516 | 4zd | 402, 422* 423*, 424*, 451 496 |
| | Neg. | 4nl | 508 | 4nm | 520 | 4nd | 448, 455, 479 |
| 51.8 | Pos. | 5pl | 476, 507 | 5pm | 466, 523 | 5pd | 444, 460, 495 |
| | Zero | 5zl | 472, 506 | 5zm | 485, 494, 515 | 5zd | 403 427*, 428*, 440* 452 |
| | Neg. | 5nl | 480, 505 | 5nm | 519 | 5nd | 447, 456, 493 |
| 67.8 | Pos. | 6pl | 467, 504 | 6pm | 477, 522 | 6pd | 445, 461, 492 |
| | Zero | 6zl | 434*, 473 | 6zm | 404 432, 586, 503 514 | 6zd | 425*, 426*, 435*, 436*, 437*, 458*, 439*, 453, 491 |
| | Neg. | | | 6nm | 481, 502, 518 | 6nd | 446, 457, 490 |
| 83.8 | Zero | | | | | 7zd | 405 429*, 430*, 441* |

* tests which included internal cycling or a non-typical loading path

## APPENDIX III. - TABLE II

INITIAL AND FINAL CONFIGURATION DATA

| Test Number | Group Symbol | Initial Conditions | | | Conditions at Failure | | |
|---|---|---|---|---|---|---|---|
| | | Void Ratio $e_o$ | Relative Density $RD_o$ (%) | Tilt Angle $\psi_o$ (deg.) | Void Ratio $e_f$ | Relative Density $RD_f$ (%) | Tilt Angle $\psi_f$ (deg.) |
| 401 | 3zd | 0.728 | 78 | 0.04 | 0.752 | 70 | -0.38 |
| 402 | 4zd | 0.722 | 80 | 0.23 | 0.740 | 74 | -0.37 |
| 403 | 5zd | 0.743 | 73 | -0.11 | 0.750 | 71 | -0.80 |
| 404 | 6zm | 0.769 | 65 | -0.30 | 0.774 | 63 | -1.19 |
| 405 | 7zd | 0.750 | 71 | -0.11 | 0.762 | 67 | -0.92 |
| 421* | 4zm | 0.766 | 66 | 0.05 | 0.783 | 60 | -0.94 |
| 422* | 4zd | 0.729 | 78 | -0.16 | 0.759 | 68 | -0.88 |
| 423* | 4zd | 0.730 | 77 | 0.07 | 0.755 | 69 | -0.59 |
| 424* | 4zd | 0.756 | 69 | -0.30 | 0.782 | 60 | -1.07 |
| 425* | 6zd | 0.728 | 78 | 0.01 | 0.748 | 71 | -0.58 |
| 426* | 6zd | 0.753 | 70 | -0.34 | 0.764 | 66 | -1.39 |
| 427* | 5zd | 0.750 | 71 | -0.33 | 0.772 | 64 | -0.89 |
| 428* | 5zd | 0.750 | 71 | -0.09 | 0.770 | 64 | -0.70 |
| 429* | 7zd | 0.714 | 83 | -0.44 | 0.735 | 76 | -0.94 |
| 430* | 7zd | 0.715 | 82 | 0.16 | 0.733 | 76 | -0.29 |
| 431 | 4zl | 0.877 | 29 | -0.05 | 0.887 | 26 | -0.49 |
| 432 | 6zm | 0.854 | 37 | -0.10 | 0.855 | 36 | -0.51 |
| 433* | 4zl | 0.923 | 14 | -0.07 | 0.908 | 19 | -0.72 |
| 434* | 6zl | 0.924 | 13 | -0.23 | 0.903 | 20 | -0.61 |
| 435* | 6zd | 0.741 | 74 | -0.48 | 0.764 | 66 | -1.00 |
| 436* | 6zd | 0.729 | 78 | -0.44 | 0.754 | 70 | -0.92 |
| 437* | 6zd | 0.734 | 76 | -0.34 | 0.750 | 71 | -0.83 |
| 438* | 6zd | 0.727 | 78 | -0.21 | 0.747 | 72 | -0.79 |
| 439* | 6zd | 0.719 | 81 | 0.25 | 0.742 | 73 | -0.30 |
| 440* | 5zd | 0.729 | 78 | 0.09 | 0.753 | 70 | -0.63 |
| 441* | 7zd | 0.723 | 80 | -0.25 | 0.747 | 72 | -0.81 |
| 442 | 3pd | 0.693 | 90 | 1.30 | 0.726 | 79 | 0.71 |
| 443 | 4pd | 0.723 | 80 | 1.53 | 0.744 | 73 | 0.55 |
| 444 | 5pd | 0.675 | 96 | 1.74 | 0.691 | 90 | 1.07 |
| 445 | 6pd | 0.687 | 92 | 1.62 | 0.698 | 88 | 1.01 |
| 446 | 6nd | 0.690 | 91 | -1.59 | 0.706 | 85 | -1.72 |
| 447 | 5nd | 0.685 | 92 | -1.70 | 0.704 | 86 | -1.80 |
| 448 | 4nd | 0.681 | 94 | -1.64 | 0.699 | 88 | -1.70 |
| 449 | 3nd | 0.669 | 98 | -1.63 | 0.693 | 90 | -1.72 |
| 450 | 3zd | 0.726 | 79 | -0.24 | 0.743 | 73 | -0.64 |
| 451 | 4zd | 0.742 | 73 | 0.11 | 0.754 | 70 | -0.66 |

* tests which included internal cycling or non-typical loading path

APPENDIX III. - TABLE II (continued)

INITIAL AND FINAL CONFIGURATION DATA

| Test Number | Group Symbol | Initial Conditions | | | Conditions at Failure | | |
|---|---|---|---|---|---|---|---|
| | | Void Ratio $e_o$ | Relative Density $RD_o$ (%) | Tilt Angle $\psi_o$ (deg.) | Void Ratio $e_f$ | Relative Density $RD_f$ (%) | Tilt Angle $\psi_f$ (deg.) |
| 452 | 5zd | 0.712 | 83 | -0.16 | 0.734 | 76 | -0.52 |
| 453 | 6zd | 0.716 | 82 | -0.16 | 0.721 | 80 | -0.57 |
| 454 | 3nd | 0.663 | 100 | -1.67 | 0.684 | 93 | -1.77 |
| 455 | 4nd | 0.688 | 91 | -1.57 | 0.706 | 85 | -1.69 |
| 456 | 5nd | 0.703 | 86 | -1.47 | 0.720 | 81 | -1.62 |
| 457 | 6nd | 0.681 | 94 | -1.78 | 0.687 | 92 | -1.77 |
| 458 | 3pd | 0.702 | 87 | 1.37 | 0.720 | 81 | 0.77 |
| 459 | 4pd | 0.678 | 95 | 1.33 | 0.697 | 88 | 0.90 |
| 460 | 5pd | 0.716 | 82 | 1.61 | 0.727 | 78 | 0.90 |
| 461 | 6pd | 0.722 | 80 | 1.52 | 0.736 | 75 | 0.64 |
| 462 | 1zd | 0.729 | 78 | -0.30 | 0.746 | 72 | -0.64 |
| 463 | 2zd | 0.718 | 81 | -0.04 | 0.733 | 76 | -0.44 |
| 464 | 3pm | 0.850 | 38 | 1.16 | 0.858 | 35 | 0.40 |
| 465 | 4pm | 0.850 | 38 | 1.45 | 0.854 | 37 | 0.57 |
| 466 | 5pl | 0.865 | 33 | 1.69 | 0.858 | 35 | 1.14 |
| 467 | 6pl | 0.965 | 0 | 1.77 | 0.916 | 16 | 1.33 |
| 468 | 3zl | 0.895 | 23 | -0.12 | 0.885 | 26 | -0.51 |
| 469 | 4zl | 0.903 | 20 | -0.29 | 0.894 | 23 | -0.60 |
| 470 | 3zl | 0.874 | 30 | -0.02 | 0.884 | 27 | -0.27 |
| 471 | 4zl | 0.902 | 21 | 0.04 | 0.898 | 22 | -0.21 |
| 472 | 5zl | 0.900 | 21 | 0.07 | 0.894 | 23 | -0.34 |
| 473 | 6zl | 0.922 | 14 | -0.15 | 0.896 | 23 | -0.56 |
| 474 | 3pm | 0.807 | 52 | 1.73 | 0.823 | 47 | 1.30 |
| 475 | 4pm | 0.809 | 51 | 1.73 | 0.826 | 46 | 1.04 |
| 476 | 5pl | 0.929 | 12 | 1.67 | 0.890 | 25 | 0.83 |
| 477 | 6pm | 0.797 | 55 | 1.73 | 0.808 | 52 | 0.72 |
| 478 | 3nm | 0.858 | 35 | -1.54 | 0.879 | 28 | -1.50 |
| 479 | 4nd | 0.755 | 69 | -1.79 | 0.775 | 63 | -1.86 |
| 480 | 5nl | 0.866 | 33 | -1.78 | 0.866 | 33 | -1.73 |
| 481 | 6nm | 0.838 | 42 | -1.80 | 0.843 | 40 | 1.71 |
| 482 | 2zm | 0.815 | 49 | -0.04 | 0.828 | 45 | -0.55 |
| 483 | 3zm | 0.841 | 41 | -0.01 | 0.840 | 41 | -0.50 |
| 484 | 4zm | 0.826 | 46 | -0.12 | 0.827 | 45 | -0.70 |
| 485 | 5zm | 0.840 | 41 | -0.25 | 0.834 | 43 | -0.87 |
| 486 | 6zm | 0.796 | 56 | -0.10 | 0.806 | 52 | -0.77 |
| 490 | 6nd | 0.728 | 78 | -1.43 | 0.751 | 70 | -1.43 |

APPENDIX III. - TABLE II (concluded)

INITIAL AND FINAL CONFIGURATION DATA

| Test Number | Group Symbol | Initial Conditions | | | Conditions at Failure | | |
|---|---|---|---|---|---|---|---|
| | | Void Ratio $e_o$ | Relative Density $RD_o$ (%) | Tilt Angle $\psi_o$ (deg.) | Void Ratio $e_f$ | Relative Density $RD_f$ (%) | Tilt Angle $\psi_f$ (deg.) |
| 491 | 6zd | 0.719 | 81 | -0.26 | 0.742 | 73 | -0.71 |
| 492 | 6pd | 0.750 | 71 | 1.06 | 0.762 | 67 | -0.52 |
| 493 | 5nd | 0.741 | 74 | -0.94 | 0.762 | 67 | -1.27 |
| 494 | 5zm | 0.774 | 63 | -0.19 | 0.779 | 61 | -0.99 |
| 495 | 5pd | 0.739 | 74 | 1.20 | 0.750 | 71 | 0.17 |
| 496 | 4zd | 0.729 | 78 | -0.16 | 0.752 | 70 | -0.57 |
| 497 | 4zm | 0.777 | 62 | -0.09 | 0.790 | 58 | -1.05 |
| 498 | 4pd | 0.754 | 70 | 1.39 | 0.767 | 65 | 0.61 |
| 499 | 3nm | 0.774 | 63 | -1.07 | 0.786 | 59 | -1.40 |
| 500 | 3zd | 0.745 | 72 | 0.11 | 0.762 | 67 | -0.34 |
| 501 | 3pd | 0.753 | 70 | 0.97 | 0.776 | 62 | -0.04 |
| 502 | 6nm | 0.849 | 38 | -1.27 | 0.846 | 39 | -1.26 |
| 503 | 6zm | 0.859 | 35 | 0.20 | 0.859 | 35 | -0.15 |
| 504 | 6pl | 0.868 | 32 | 0.95 | 0.861 | 34 | 0.32 |
| 505 | 5nl | 0.885 | 26 | -1.40 | 0.880 | 28 | -1.42 |
| 506 | 5zl | 0.900 | 21 | -0.20 | 0.888 | 25 | -0.78 |
| 507 | 5pl | 0.887 | 26 | 1.33 | 0.876 | 29 | 0.65 |
| 508 | 4nl | 0.876 | 29 | -1.42 | 0.873 | 30 | -1.35 |
| 509 | 4zl | 0.893 | 24 | -0.22 | 0.888 | 25 | -0.63 |
| 510 | 4pl | 0.919 | 15 | 1.15 | 0.900 | 21 | 0.26 |
| 511 | 3nl | 0.876 | 29 | -1.35 | 0.878 | 29 | -1.33 |
| 512 | 3zl | 0.877 | 29 | -0.12 | 0.883 | 27 | -0.50 |
| 513 | 3pl | 0.890 | 25 | 0.89 | 0.889 | 25 | 0.27 |
| 514 | 6zm | 0.825 | 46 | 0.11 | 0.818 | 48 | -0.42 |
| 515 | 5zm | 0.836 | 42 | 0.07 | 0.833 | 43 | -0.70 |
| 516 | 4zm | 0.812 | 50 | 0.13 | 0.815 | 49 | -0.46 |
| 517 | 3zm | 0.808 | 52 | 0.17 | 0.823 | 47 | -0.52 |
| 518 | 6nm | 0.821 | 47 | -1.23 | 0.819 | 48 | -0.89 |
| 519 | 5nm | 0.814 | 50 | -1.11 | 0.818 | 48 | -1.57 |
| 520 | 4nm | 0.823 | 47 | -1.29 | 0.834 | 43 | -1.42 |
| 521 | 3nm | 0.826 | 46 | -1.08 | 0.836 | 42 | -1.13 |
| 522 | 6pm | 0.833 | 43 | 1.17 | 0.821 | 47 | -0.36 |
| 523 | 5pm | 0.820 | 48 | 0.85 | 0.823 | 47 | -0.65 |
| 524 | 4pm | 0.808 | 52 | 0.94 | 0.809 | 51 | 0.08 |
| 525 | 3pm | 0.796 | 56 | 1.67 | 0.810 | 51 | 0.19 |

## APPENDIX III. - TABLE III

### DISPLACEMENT INCREMENTS AND FORCES AT FAILURE

| Test Number | Group Symbol | Normal Force N (kg) | Shear Force T (kg) | Moment M (cm-kg) | Vertical Displacement Increment $\Delta\delta_N$ (cm) | Horizontal Displacement Increment $\Delta\delta_T$ (cm) | Rotation Increment $\Delta\psi$ (rad) |
|---|---|---|---|---|---|---|---|
| 401 | 3zd | 19.8 | 22.0 | 3.9 | -0.00445 | 0.01270 | -0.00113 |
| 402 | 4zd | 35.8 | 39.2 | 7.3 | -0.00427 | 0.01270 | -0.00107 |
| 403 | 5zd | 51.8 | 54.8 | 23.5 | -0.00763 | 0.02540 | -0.00243 |
| 404 | 6zm | 67.8 | 69.6 | 46.4 | -0.00340 | 0.01270 | -0.00071 |
| 405 | 7zd | 83.8 | 81.6 | 45.4 | -0.00320 | 0.01270 | -0.00088 |
| 421* | 4zm | 35.8 | 37.8 | 18.6 | -0.00358 | 0.01270 | -0.00112 |
| 422* | 4zd | 35.8 | 38.4 | 17.4 | -0.00394 | 0.01270 | -0.00092 |
| 423* | 4zd | 35.8 | 37.3 | 11.7 | -0.00374 | 0.01270 | -0.00095 |
| 424* | 4zd | 35.8 | 36.6 | 20.2 | -0.00406 | 0.01270 | -0.00082 |
| 425* | 6zd | 67.8 | 69.3 | 22.6 | -0.00774 | 0.02540 | -0.00164 |
| 426* | 6zd | 67.8 | 66.6 | 54.1 | -0.00519 | 0.02540 | -0.00123 |
| 427* | 5zd | 51.8 | 51.4 | 26.2 | -0.00722 | 0.02540 | -0.00189 |
| 428* | 5zd | 51.8 | 52.6 | 20.6 | -0.00722 | 0.02540 | -0.00187 |
| 429* | 7zd | 83.8 | 81.6 | 46.4 | -0.00765 | 0.02540 | -0.00099 |
| 430* | 7zd | 83.8 | 76.2 | 14.3 | -0.00735 | 0.02540 | -0.00175 |
| 431 | 4zl | 35.8 | 27.4 | 9.7 | -0.00310 | 0.02540 | -0.00061 |
| 432 | 6zm | 67.8 | 51.6 | 19.8 | -0.00364 | 0.02540 | -0.00073 |
| 433* | 4zl | 35.8 | 26.4 | 14.2 | -0.00119 | 0.02540 | -0.00083 |
| 434* | 6zl | 67.8 | 47.8 | 23.8 | -0.00184 | 0.02540 | -0.00049 |
| 435* | 6zd | 67.8 | 66.5 | 38.9 | -0.00770 | 0.02540 | -0.00116 |
| 436* | 6zd | 67.8 | 67.0 | 35.8 | -0.00762 | 0.02540 | -0.00125 |
| 437* | 6zd | 67.8 | 68.0 | 32.3 | -0.00750 | 0.02540 | -0.00124 |
| 438* | 6zd | 67.8 | 66.4 | 30.7 | -0.00855 | 0.02920 | -0.00174 |
| 439* | 6zd | 67.8 | 65.4 | 11.7 | -0.00712 | 0.02540 | -0.00161 |
| 440* | 5zd | 51.8 | 51.6 | 18.5 | -0.00695 | 0.02540 | -0.00162 |
| 441* | 7zd | 83.8 | 79.9 | 40.0 | -0.00717 | 0.02540 | -0.00126 |
| 442 | 3pd | 19.8 | 20.2 | -7.3 | -0.00214 | 0.00635 | -0.00053 |
| 443 | 4pd | 35.8 | 33.2 | -10.9 | -0.00339 | 0.01270 | -0.00146 |
| 444 | 5pd | 51.8 | 44.5 | -31.4 | -0.00169 | 0.00635 | -0.00055 |
| 445 | 6pd | 67.8 | 57.0 | -39.3 | -0.00196 | 0.00635 | -0.00072 |
| 446 | 6nd | 67.8 | 69.6 | 66.0 | -0.00233 | 0.00635 | -0.00003 |
| 447 | 5nd | 51.8 | 53.9 | 53.0 | -0.00246 | 0.00635 | -0.00002 |
| 448 | 4nd | 35.8 | 39.9 | 33.7 | -0.00298 | 0.00635 | -0.00007 |
| 449 | 3nd | 19.8 | 24.2 | 17.7 | -0.00300 | 0.00635 | +0.00004 |
| 450 | 3zd | 19.8 | 21.5 | 6.6 | -0.00170 | 0.00508 | -0.00022 |
| 451 | 4zd | 35.8 | 36.6 | 13.1 | -0.00113 | 0.00508 | -0.00035 |

* tests which included internal cycling or non-typical loading path

APPENDIX III. - TABLE III (continued)

DISPLACEMENT INCREMENTS AND FORCES AT FAILURE

| Test Number | Group Symbol | Normal Force N (kg) | Shear Force T (kg) | Moment M (cm-kg) | Vertical Displacement Increment $\Delta\delta_N$ (cm) | Horizontal Displacement Increment $\Delta\delta_T$ (cm) | Rotation Increment $\Delta\psi$ (rad) |
|---|---|---|---|---|---|---|---|
| 452 | 5zd | 51.8 | 52.5 | 15.3 | -0.00174 | 0.00508 | -0.00029 |
| 453 | 6zd | 67.8 | 63.8 | 22.2 | -0.00139 | 0.00508 | -0.00029 |
| 454 | 3nd | 19.8 | 23.5 | 18.2 | -0.00224 | 0.00508 | -0.00003 |
| 455 | 4nd | 35.8 | 37.5 | 33.4 | -0.00196 | 0.00508 | -0.00005 |
| 456 | 5nd | 51.8 | 53.4 | 47.6 | -0.00181 | 0.00508 | -0.00005 |
| 457 | 6nd | 67.8 | 69.4 | 69.0 | -0.00186 | 0.00508 | -0.00004 |
| 458 | 3pd | 19.8 | 20.3 | -7.9 | -0.00128 | 0.00508 | -0.00038 |
| 459 | 4pd | 35.8 | 33.4 | -17.8 | -0.00152 | 0.00508 | -0.00044 |
| 460 | 5pd | 51.8 | 43.5 | -26.4 | -0.00140 | 0.00508 | -0.00045 |
| 461 | 6pd | 67.8 | 58.4 | -24.9 | -0.00131 | 0.00508 | -0.00057 |
| 462 | 1zd | 7.8 | 9.4 | 2.0 | -0.00195 | 0.00508 | -0.00041 |
| 463 | 2zd | 11.8 | 13.1 | 2.4 | -0.00190 | 0.00508 | -0.00039 |
| 464 | 3pm | 19.8 | 14.4 | -4.1 | -0.00088 | 0.00508 | -0.00036 |
| 465 | 4pm | 35.8 | 24.8 | -11.3 | -0.00058 | 0.00508 | -0.00045 |
| 466 | 5pl | 51.8 | 32.6 | -33.6 | -0.00017 | 0.00508 | -0.00038 |
| 467 | 6pl | 67.8 | 34.6 | -51.8 | +0.00035 | 0.00508 | -0.00033 |
| 468 | 3zl | 19.8 | 13.1 | 5.2 | +0.00008 | 0.00508 | -0.00024 |
| 469 | 4zl | 35.8 | 24.9 | 11.8 | -0.00010 | 0.00508 | -0.00014 |
| 470 | 3zl | 19.8 | 15.0 | 2.8 | -0.00366 | 0.02540 | -0.00105 |
| 471 | 4zl | 35.8 | 25.1 | 4.2 | -0.00198 | 0.02540 | -0.00111 |
| 472 | 5zl | 51.8 | 37.5 | 10.0 | -0.00099 | 0.01270 | -0.00033 |
| 473 | 6zl | 67.8 | 45.6 | 21.8 | -0.00047 | 0.01270 | -0.00030 |
| 474 | 3pm | 19.8 | 15.5 | -13.4 | -0.00528 | 0.02540 | -0.00204 |
| 475 | 4pm | 35.8 | 28.6 | -20.6 | -0.00493 | 0.02540 | -0.00205 |
| 476 | 5pl | 51.8 | 32.2 | -24.4 | +0.00020 | 0.01270 | -0.00111 |
| 477 | 6pm | 67.8 | 50.2 | -28.0 | -0.00470 | 0.02540 | -0.00219 |
| 478 | 3nm | 19.8 | 16.9 | 15.4 | -0.00226 | 0.01270 | +0.00017 |
| 479 | 4nd | 35.8 | 32.2 | 36.8 | -0.00694 | 0.02540 | -0.00015 |
| 480 | 5nl | 51.8 | 39.6 | 50.8 | -0.00180 | 0.01270 | +0.00013 |
| 481 | 6nm | 67.8 | 57.5 | 66.5 | -0.00222 | 0.01270 | +0.00008 |
| 482 | 2zm | 11.8 | 11.5 | 3.0 | -0.00288 | 0.01270 | -0.00092 |
| 483 | 3zm | 19.8 | 17.0 | 5.1 | -0.00206 | 0.01270 | -0.00092 |
| 484 | 4zm | 35.8 | 30.3 | 13.8 | -0.00226 | 0.01270 | -0.00088 |
| 485 | 5zm | 51.8 | 43.5 | 25.6 | -0.00187 | 0.01270 | -0.00074 |
| 486 | 6zm | 67.8 | 56.6 | 30.0 | -0.00189 | 0.01270 | -0.00063 |
| 490 | 6nd | 67.8 | 64.7 | 55.6 | -0.00503 | 0.01750 | -0.00012 |

APPENDIX III. - TABLE III (concluded)

DISPLACEMENT INCREMENTS AND FORCES AT FAILURE

| Test Number | Group Symbol | Normal Force N (kg) | Shear Force T (kg) | Moment M (cm-kg) | Vertical Displacement Increment $\Delta\delta_N$ (cm) | Horizontal Displacement Increment $\Delta\delta_T$ (cm) | Rotation Increment $\Delta\psi$ (rad) |
|---|---|---|---|---|---|---|---|
| 491 | 6zd | 67.8 | 69.0 | 27.6 | -0.00811 | 0.02680 | -0.00135 |
| 492 | 6pd | 67.8 | 66.1 | 20.2 | -0.00562 | 0.02540 | -0.00296 |
| 493 | 5nd | 51.8 | 51.4 | 37.3 | -0.00637 | 0.02110 | -0.00052 |
| 494 | 5zm | 51.8 | 51.1 | 29.1 | -0.00575 | 0.02670 | -0.00169 |
| 495 | 5pd | 51.8 | 48.8 | -5.0 | -0.00398 | 0.01640 | -0.00163 |
| 496 | 4zd | 35.8 | 37.4 | 11.3 | -0.00405 | 0.01270 | -0.00041 |
| 497 | 4zm | 35.8 | 37.6 | 20.8 | -0.00296 | 0.01270 | -0.00079 |
| 498 | 4pd | 35.8 | 32.6 | -12.1 | -0.00140 | 0.00635 | -0.00078 |
| 499 | 3nm | 19.8 | 20.6 | 14.4 | -0.00360 | 0.01270 | -0.00053 |
| 500 | 3zd | 19.8 | 21.6 | 3.5 | -0.00374 | 0.01270 | -0.00093 |
| 501 | 3pd | 19.8 | 20.5 | 0.4 | -0.00322 | 0.01270 | -0.00152 |
| 502 | 6nm | 67.8 | 51.0 | 49.2 | -0.00179 | 0.01270 | +0.00003 |
| 503 | 6zm | 67.8 | 49.0 | 5.8 | -0.00132 | 0.01270 | -0.00034 |
| 504 | 6pl | 67.8 | 47.4 | -12.5 | -0.00108 | 0.01270 | -0.00092 |
| 505 | 5pl | 51.8 | 39.1 | 41.8 | -0.00145 | 0.01270 | +0.00008 |
| 506 | 5zl | 51.8 | 38.2 | 23.0 | -0.00090 | 0.01270 | -0.00030 |
| 507 | 5pl | 51.8 | 34.8 | -19.1 | -0.00060 | 0.01270 | -0.00097 |
| 508 | 4nl | 35.8 | 26.2 | 26.8 | -0.00269 | 0.02540 | +0.00016 |
| 509 | 4zl | 35.8 | 26.3 | 12.5 | -0.00118 | 0.01270 | -0.00028 |
| 510 | 4pl | 35.8 | 24.6 | -5.1 | -0.00017 | 0.01270 | -0.00092 |
| 511 | 3nl | 19.8 | 14.9 | 13.7 | -0.00256 | 0.02540 | +0.00009 |
| 512 | 3zl | 19.8 | 14.9 | 5.1 | -0.00254 | 0.02540 | -0.00045 |
| 513 | 3pl | 19.8 | 14.4 | -2.8 | -0.00214 | 0.02540 | -0.00205 |
| 514 | 6zm | 67.8 | 55.5 | 16.3 | -0.00348 | 0.02540 | -0.00192 |
| 515 | 5zm | 51.8 | 43.5 | 20.6 | -0.00178 | 0.01270 | -0.00072 |
| 516 | 4zm | 35.8 | 32.0 | 9.1 | -0.00384 | 0.02540 | -0.00151 |
| 517 | 3zm | 19.8 | 17.5 | 5.3 | -0.00440 | 0.02540 | -0.00150 |
| 518 | 6nm | 67.8 | 57.3 | 34.6 | -0.00404 | 0.02540 | -0.00075 |
| 519 | 5nm | 51.8 | 46.0 | 46.2 | -0.00571 | 0.02540 | -0.00064 |
| 520 | 4nm | 35.8 | 30.3 | 28.2 | -0.00508 | 0.02540 | -0.00051 |
| 521 | 3nm | 19.8 | 18.0 | 11.6 | -0.00232 | 0.01270 | -0.00046 |
| 522 | 6pm | 67.8 | 52.9 | 14.0 | -0.00103 | 0.01270 | -0.00103 |
| 523 | 5pm | 51.8 | 43.3 | 19.1 | -0.00176 | 0.01270 | -0.00093 |
| 524 | 4pm | 35.8 | 29.0 | -1.6 | -0.00164 | 0.01270 | -0.00112 |
| 525 | 3pm | 19.8 | 18.2 | -2.0 | -0.00211 | 0.01270 | -0.00109 |

APPENDIX III. - TABLE IV

Means and Standard Deviations of
Angles Defined by Equation (21)

| Angle | Mean Value (deg.) | Standard Deviation (deg.) |
|---|---|---|
| $\theta_A$ | 39.02 | ±3.66 |
| $\theta_B$ | 12.80 | ±5.53 |
| $\theta_C$ | 26.76 | ±3.17 |
| $\theta_D$ | -3.09 | ±1.88 |
| $\theta_E$ | -4.32 | ±3.33 |
| $\theta_F$ | -1.23 | ±2.64 |
| $\theta_G$ | -38.79 | ±3.80 |
| $\theta_H$ | -12.07 | ±6.05 |
| $\theta_I$ | -26.72 | +3.21 |

TECHNICAL LIBRARY
BLDG 313
ABERDEEN PROVING GROUND MD.
STEAP-TL

## CAPTIONS FOR FIGURES


Figure 1 Yield Surface, Stress Path, and Plastic Strain Increment Vector.

Figure 2 Vertical Cross-sectional View of Direct Shear Device in the Plane of the Applied Tractions.

Figure 3 Enlarged View of a Portion of Figure 2 Illustrating Dimensions.

Figure 4 Plan View of Direct Shear Apparatus.

Figure 5 Initial Configuration of Soil Specimen and Positive Directions of Applied Tractions and Resulting Displacements.

Figure 6 Initial & Displaced Configurations of Shear Box Device.

Figure 7 Two Dimensional Projections of Loading Paths for Tests 452 and 472.

Figure 8 Two Dimensional Projections of Displacement Paths for Tests 452 and 472.

Figure 9 Graphs of Tangential Force Versus Tangential Displacement and Normal Force Versus Normal Displacement for Test 452 and 472.

Figure 10 Graph of Tangential Force Versus Relative Density and Current Tilt Angle for Tests 452 and 472.

Figure 11 Plots of Failure Force Coordinates and Displacement Increment Vector Projections for Tests Having Final Normal Loads of 19.8 kg. and 35.8 kg.

Figure 12 Plots of Failure Force Coordinates and Displacement Increment Vector Projections for Tests Having Final Normal Loads of 51.8 kg. and 67.8 kg.

Figure 13 Plot of Failure Force Coordinates and Displacement Increment Vector Projections for Tests Having a Moment at Failure between -10.1 cm.-kg. and -30.0 cm.-kg.

Figure 14 Plot of Failure Force Coordinates and Displacement Increment Vector Projections for Tests Having a Moment at Failure between +9.9 cm.-kg. and -10.0 cm.-kg.

Figure 15 Plot of Failure Force Coordinates and Displacement Increment Vector Projections for Tests Having a Moment at Failure between +29.9 cm.-kg. and +10.0 cm.-kg.

Figure 16 Plot of Failure Force Coordinates and Displacement Increment Vector Projections for Test Having a Moment at Failure between +49.9 cm.-kg. and +30.0 cm.-kg.

## CAPTIONS FOR FIGURES

Figure 17 Pictoral Identification of Vectors and Angles Defined by Equations (19) through (21).

Figure 18 Scatter Diagram of the Angle $\theta_F$ Versus the Relative Density at Failure.

Figure 19 Scatter Diagram of the Angle $\theta_F$ Versus the Angle of Tilt at Failure.

Figure 20 Scatter Diagram of the Angles $\theta_H$ and $\theta_I$ Versus the Relative Density at Failure.

Figure 21 Principal Stress Space and Failure Theories.

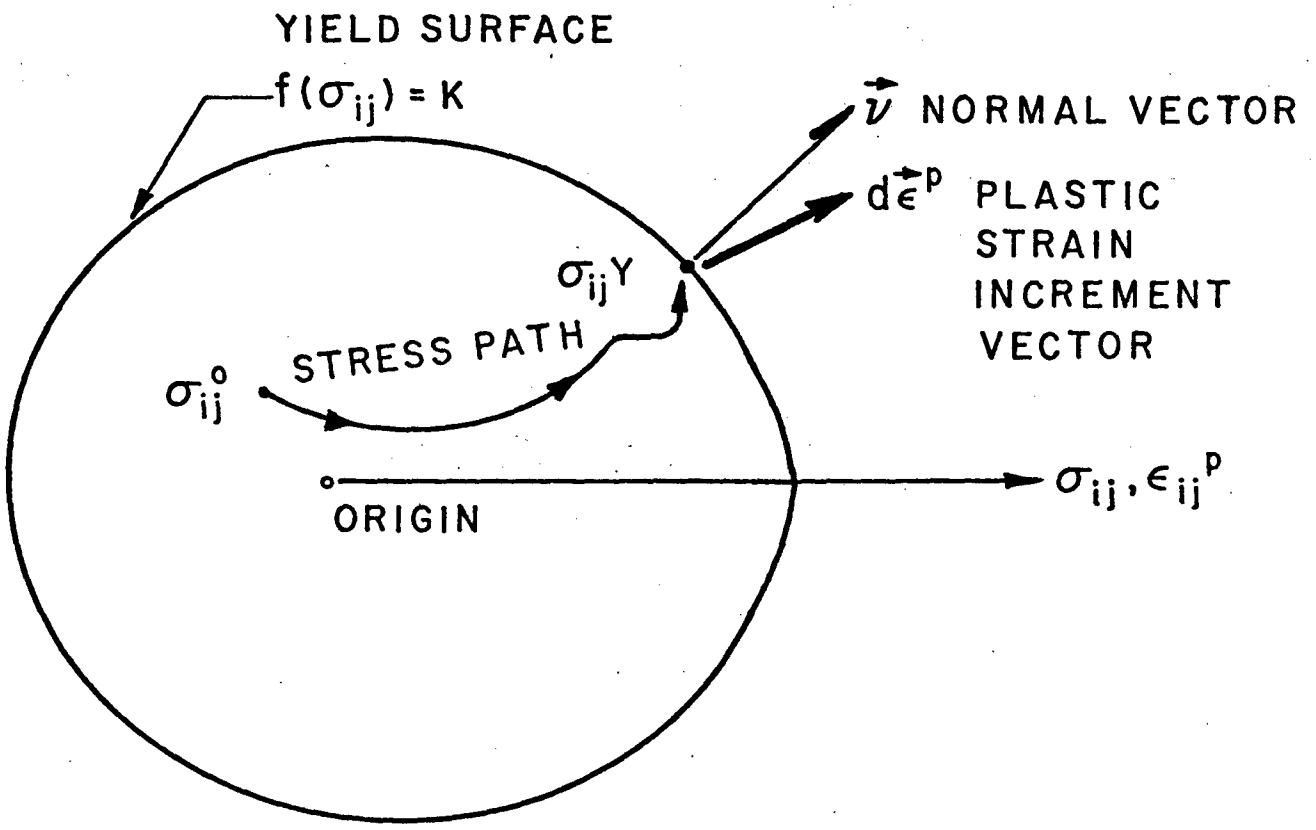


FIG. 1 YIELD SURFACE, STRESS PATH, AND PLASTIC STRAIN INCREMENT VECTOR.

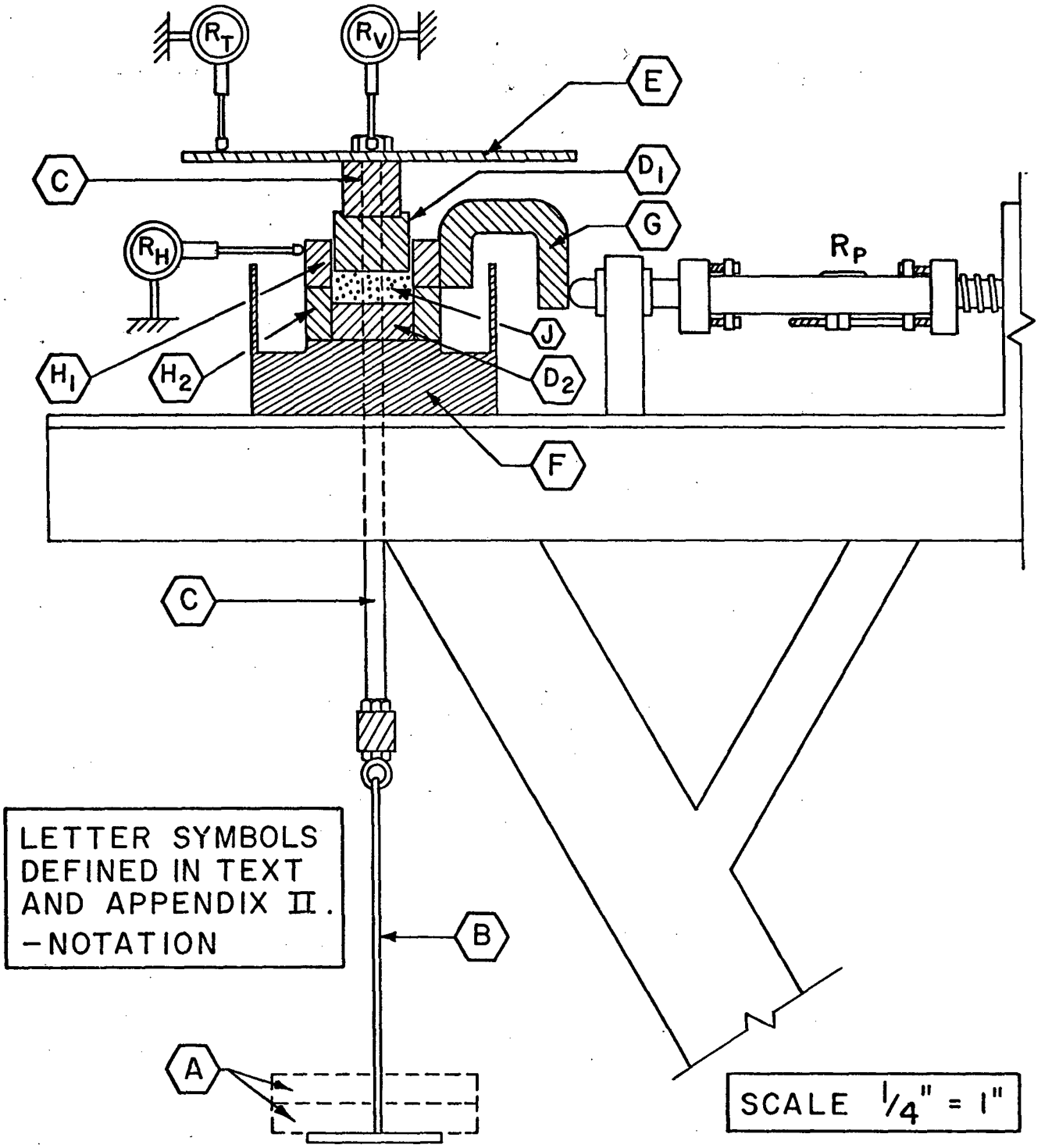


FIG. 2 VERTICAL CROSS-SECTIONAL VIEW OF DIRECT SHEAR DEVICE IN THE PLANE OF THE APPLIED TRACTIONS.

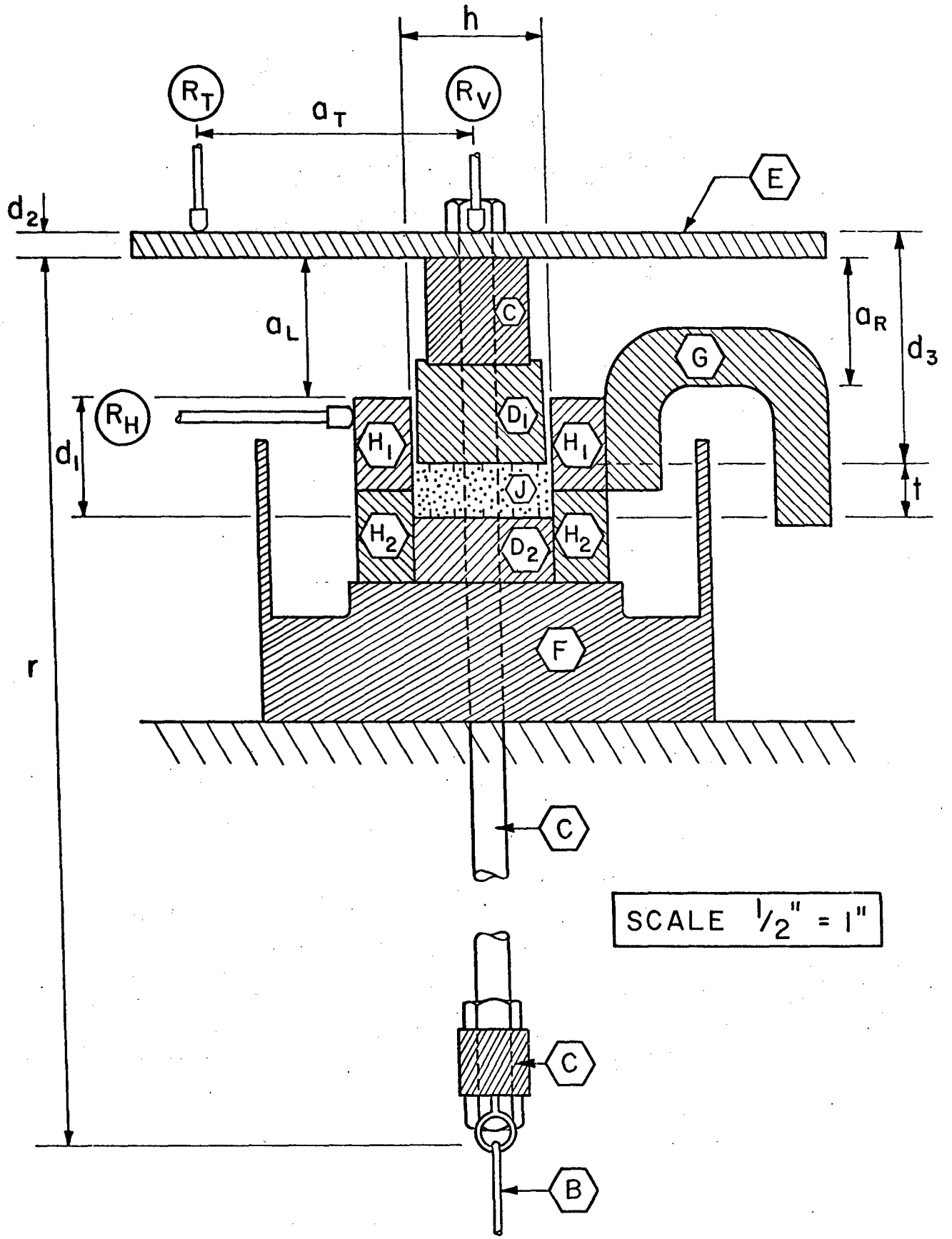


FIG. 3 ENLARGED VIEW OF A PORTION OF FIG. 2 ILLUSTRATING DIMENSIONS.

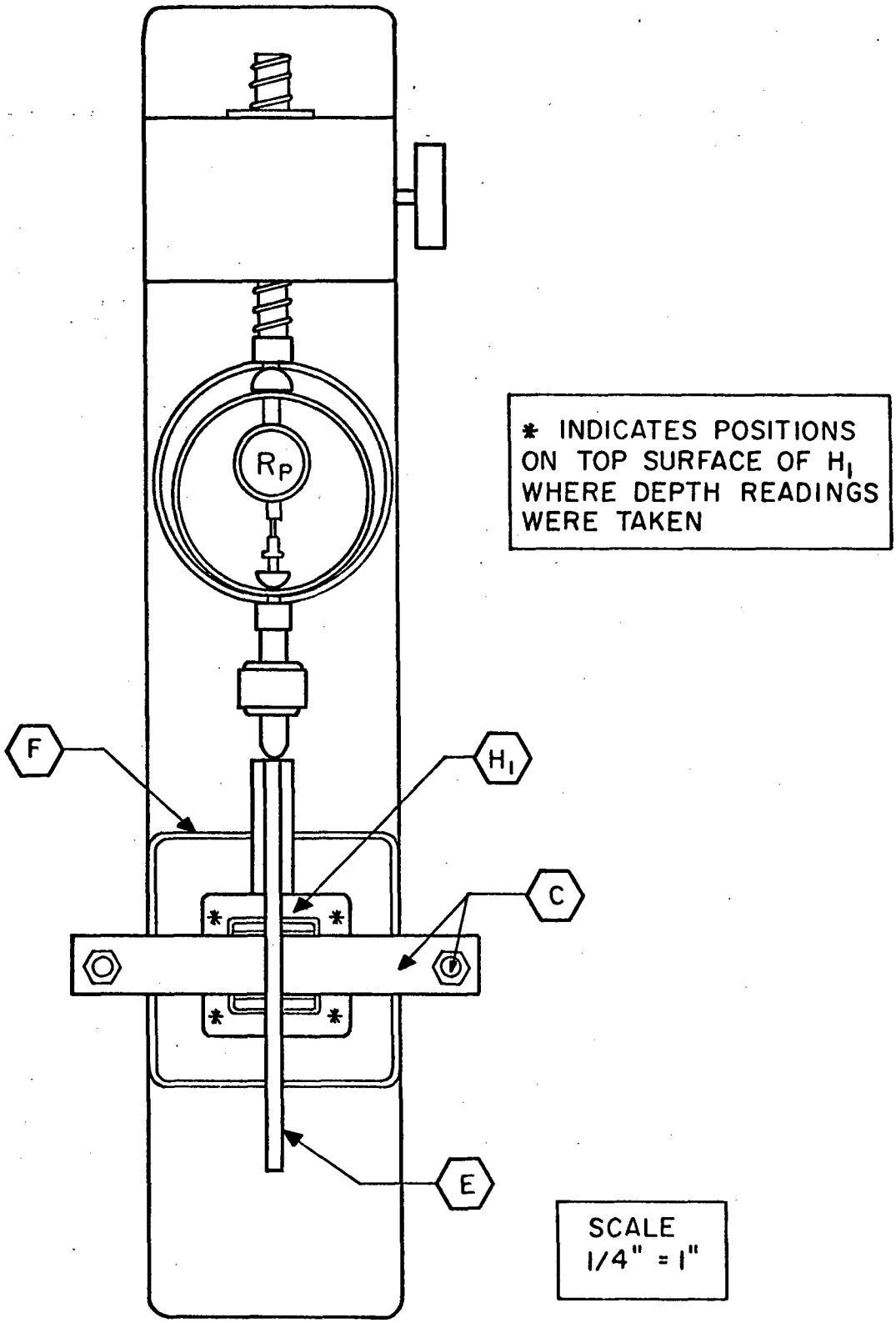


FIG. 4 PLAN VIEW OF DIRECT SHEAR APPARATUS.

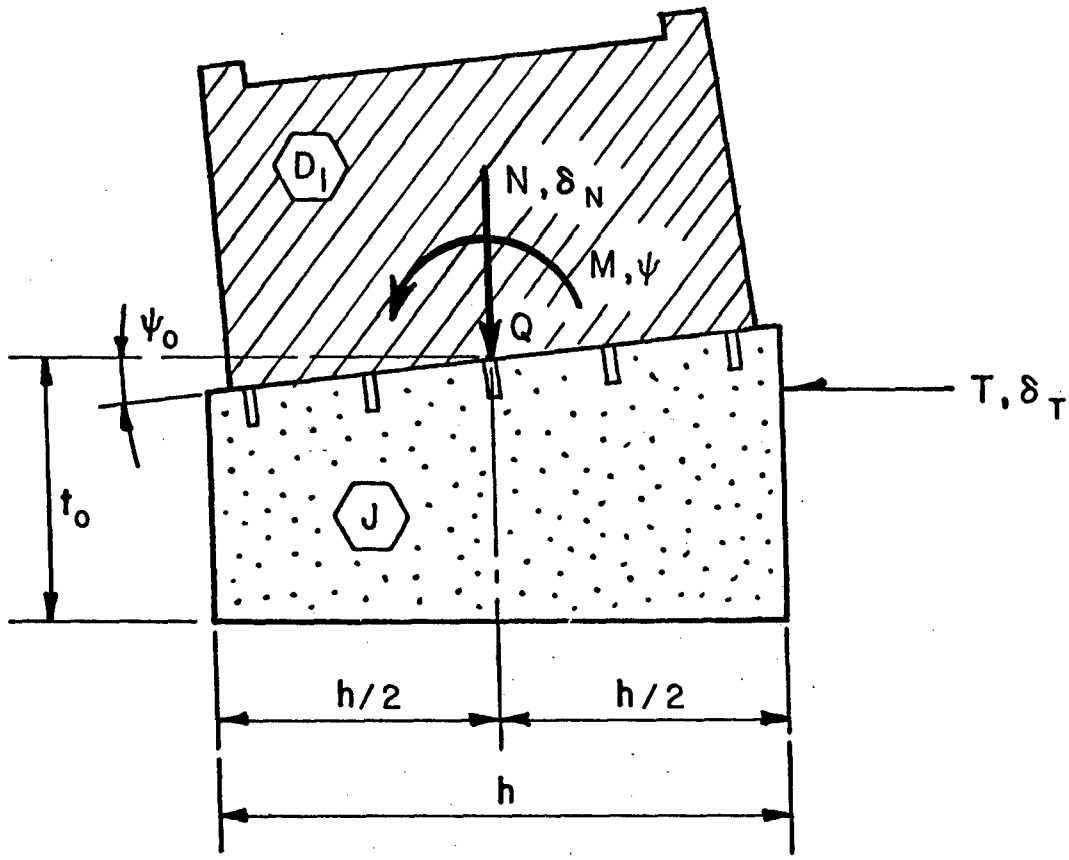


FIG. 5 INITIAL CONFIGURATION OF SOIL SPECIMEN AND POSITIVE DIRECTIONS OF APPLIED TRACTIONS AND RESULTING DISPLACEMENTS.

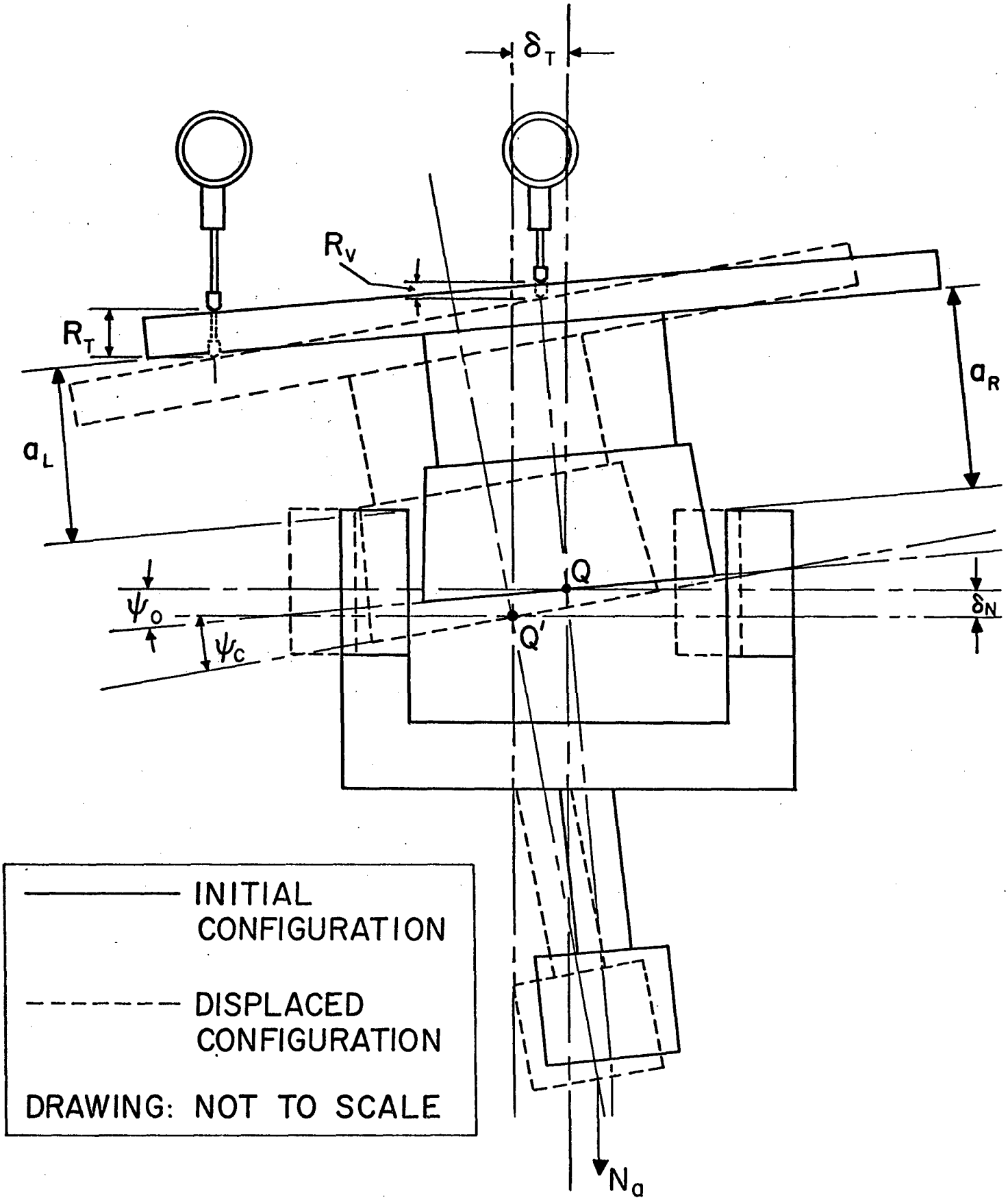


FIG. 6 INITIAL & DISPLACED CONFIGURATIONS OF SHEAR BOX DEVICE.

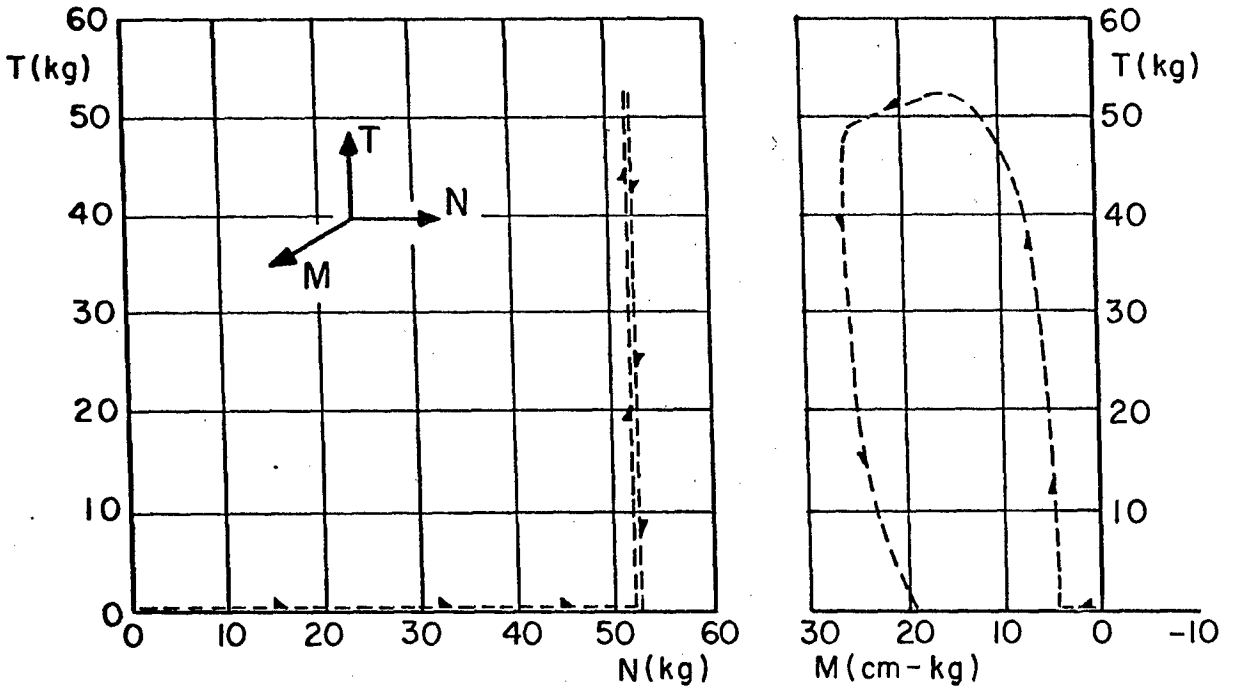


a. TEST 452, GROUP 5 zd

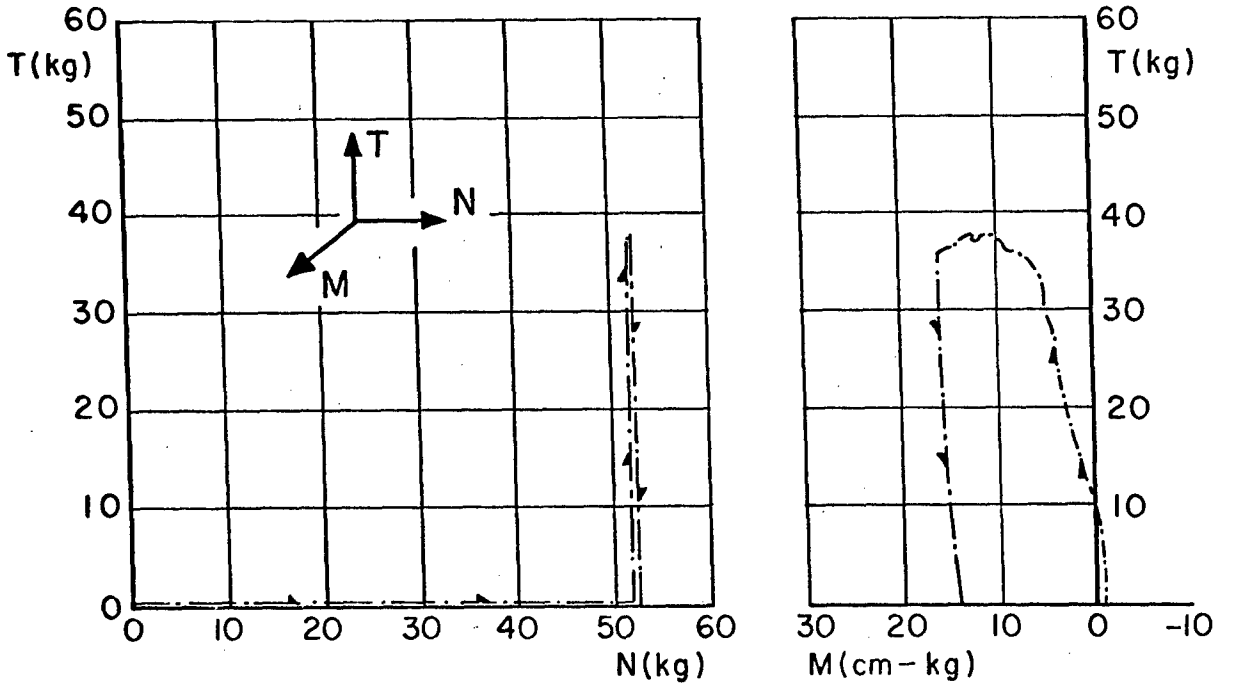


b. TEST 472, GROUP 5 zℓ

FIG. 7 TWO DIMENSIONAL PROJECTIONS OF LOADING PATHS FOR TESTS 452 AND 472.

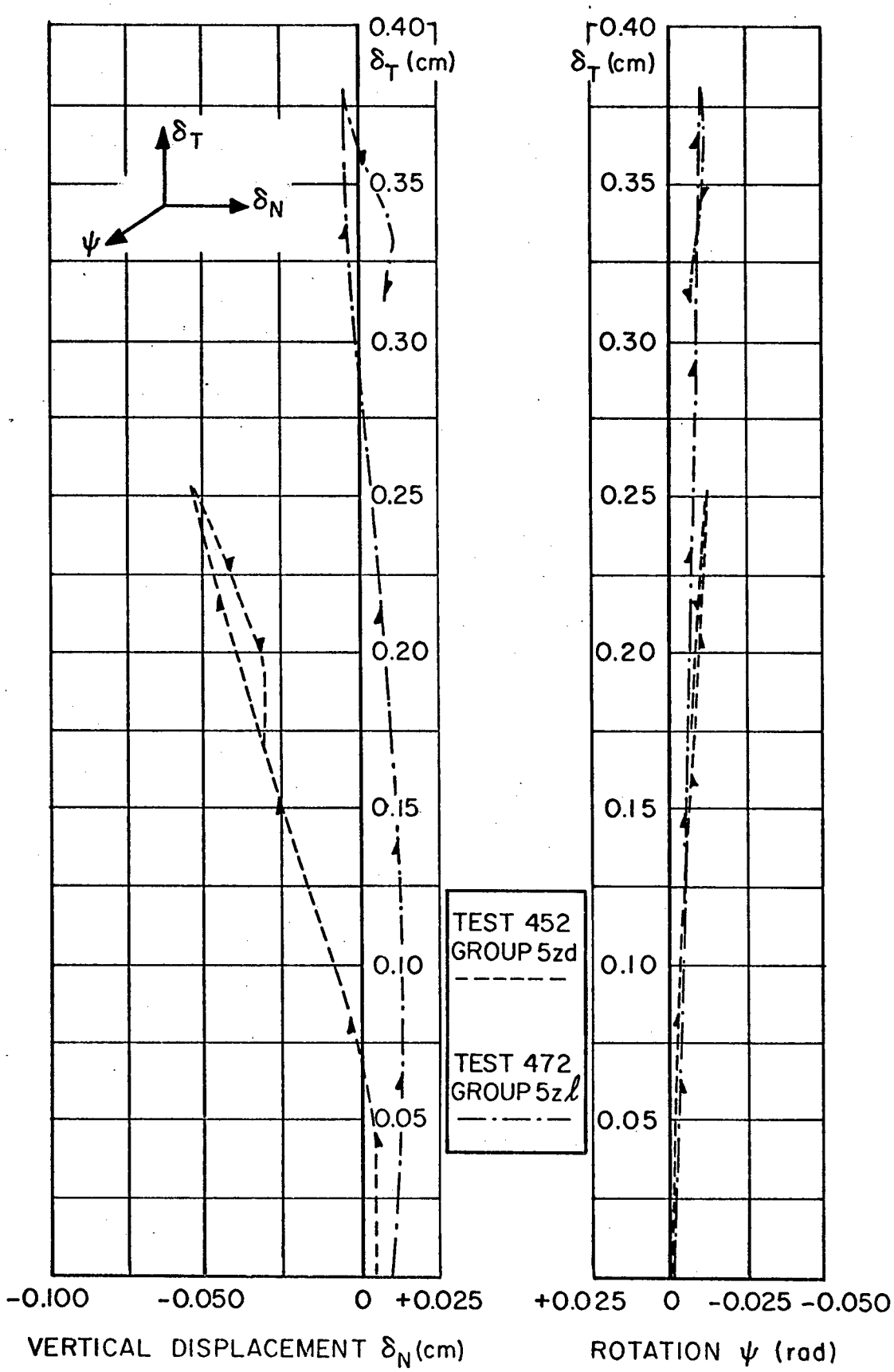


FIG. 8 TWO DIMENSIONAL PROJECTIONS OF DISPLACEMENT PATHS FOR TESTS 452 AND 472.

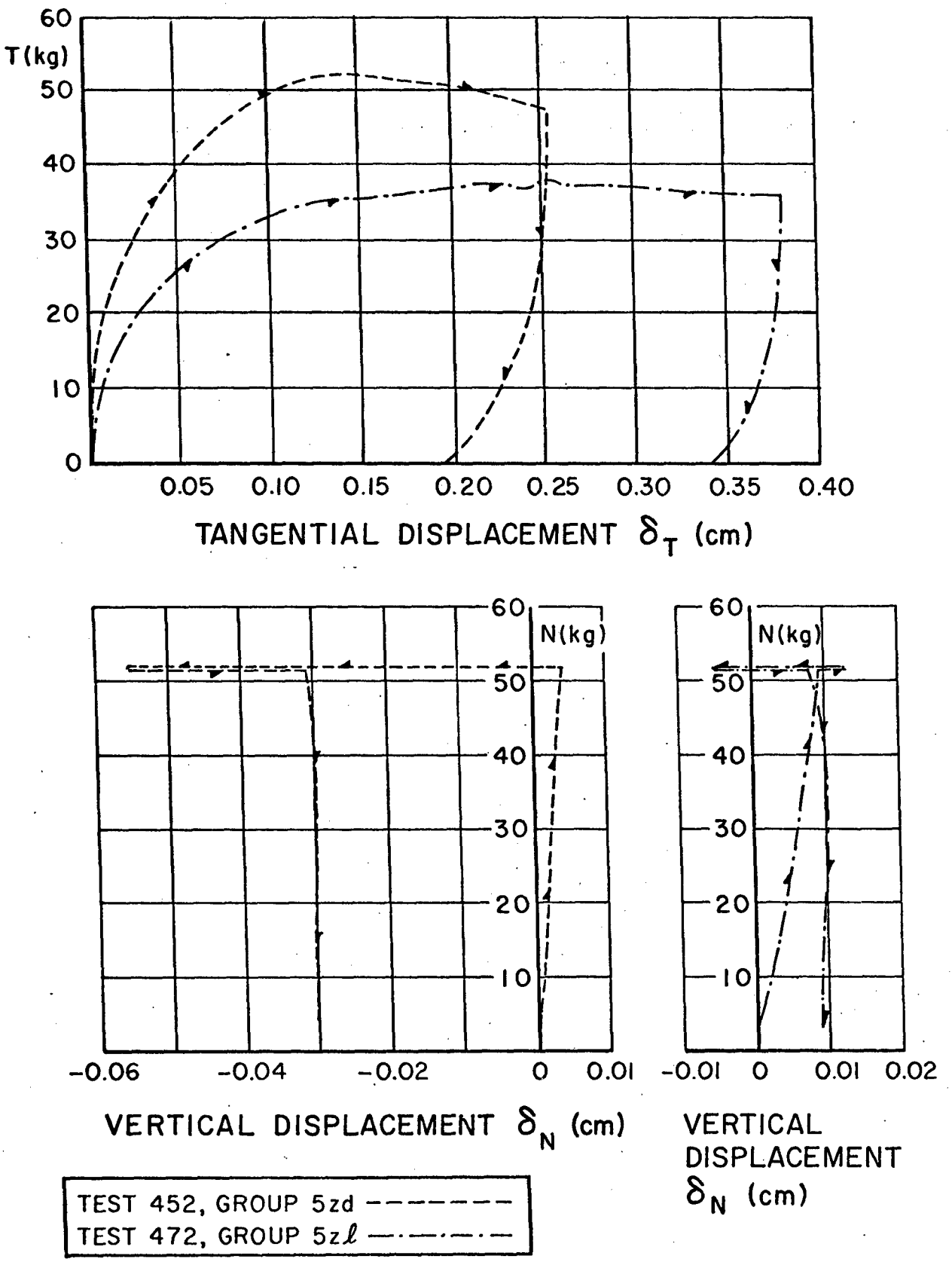


FIG. 9 GRAPHS OF TANGENTIAL FORCE VERSUS TANGENTIAL DISPLACEMENT AND NORMAL FORCE VERSUS NORMAL DISPLACEMENT FOR TEST 452 AND 472.

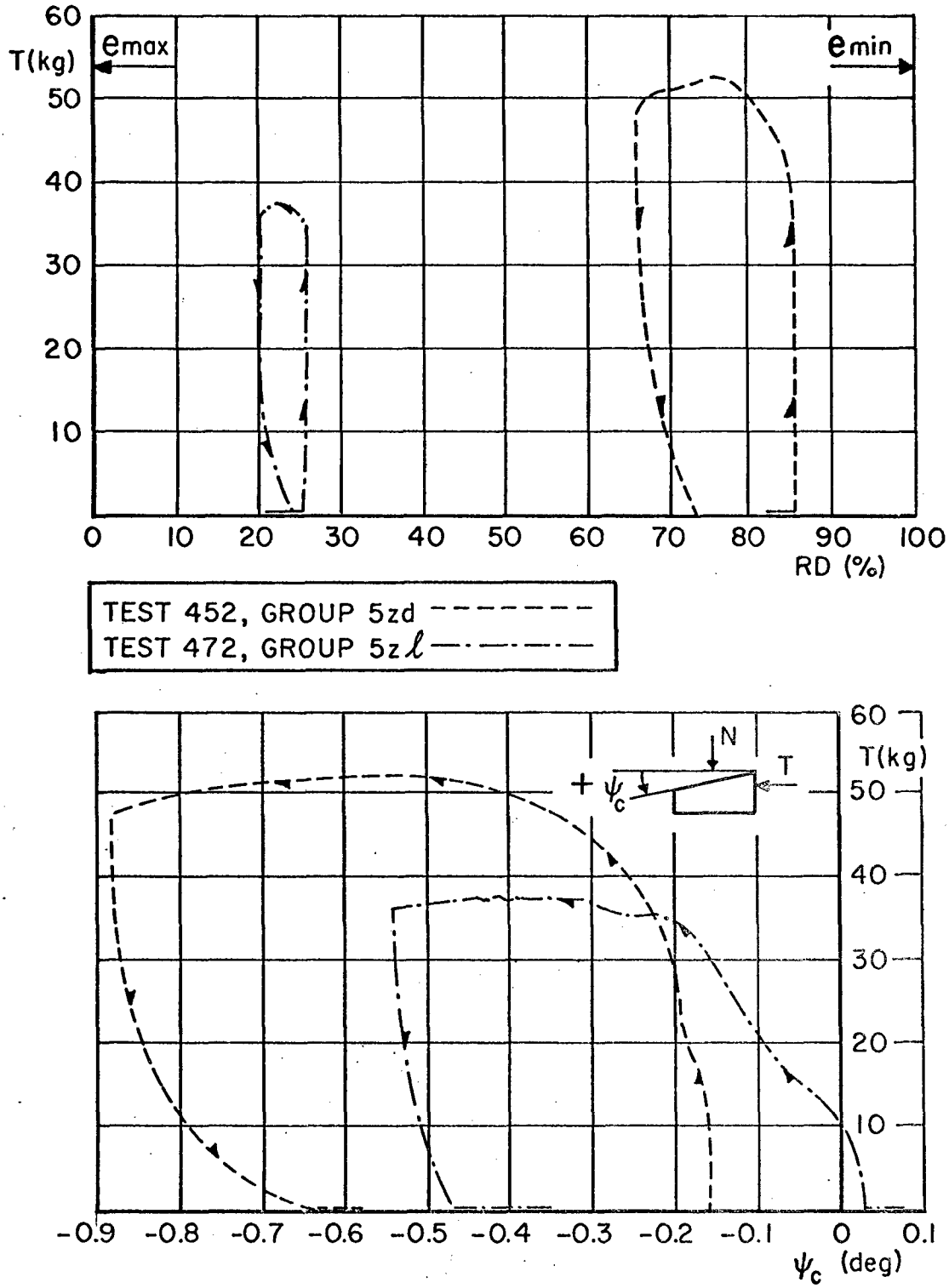


FIG. 10 GRAPH OF TANGENTIAL FORCE VERSUS RELATIVE DENSITY AND CURRENT TILT ANGLE FOR TESTS 452 AND 472.

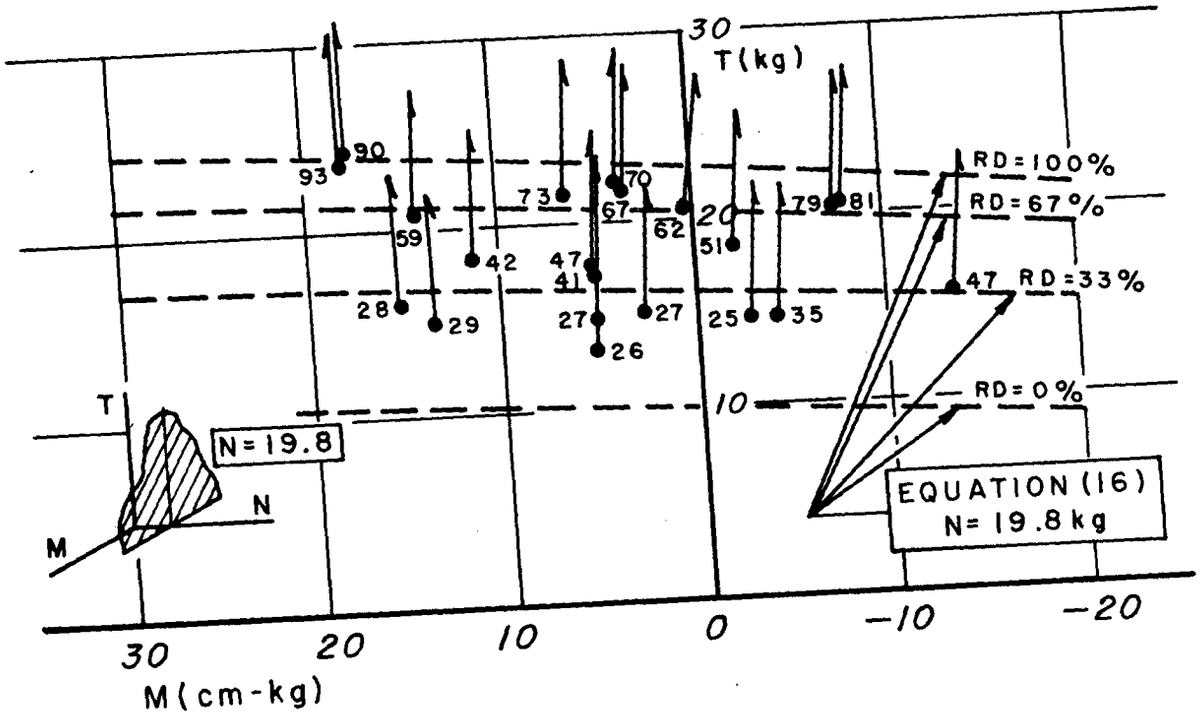


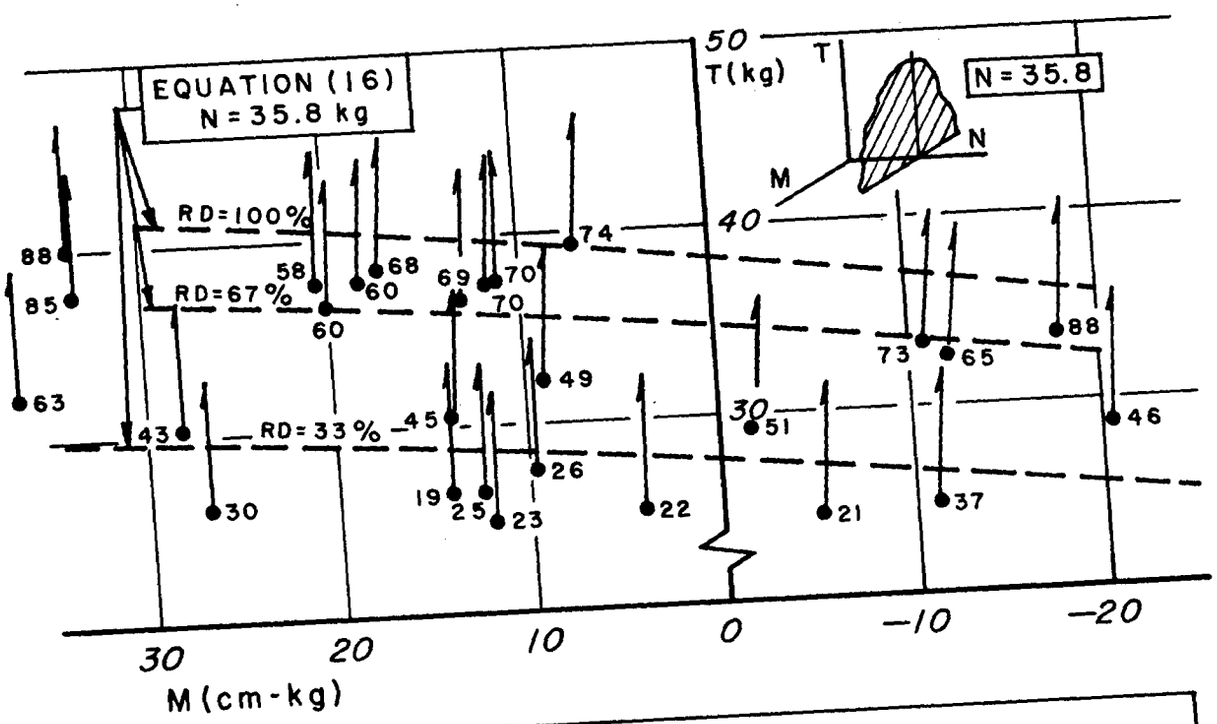


DIRECTION OF DISPLACEMENT INCREMENT VECTOR PROJECTION AT FAILURE

M,T COORDINATES OF TEST POINT AT FAILURE } 46 { RELATIVE DENSITY AT FAILURE

FIG. 11 PLOTS OF FAILURE FORCE COORDINATES AND DISPLACEMENT INCREMENT VECTOR PROJECTIONS FOR TESTS HAVING FINAL NORMAL LOADS OF 19.8 KG. AND 35.8 KG.

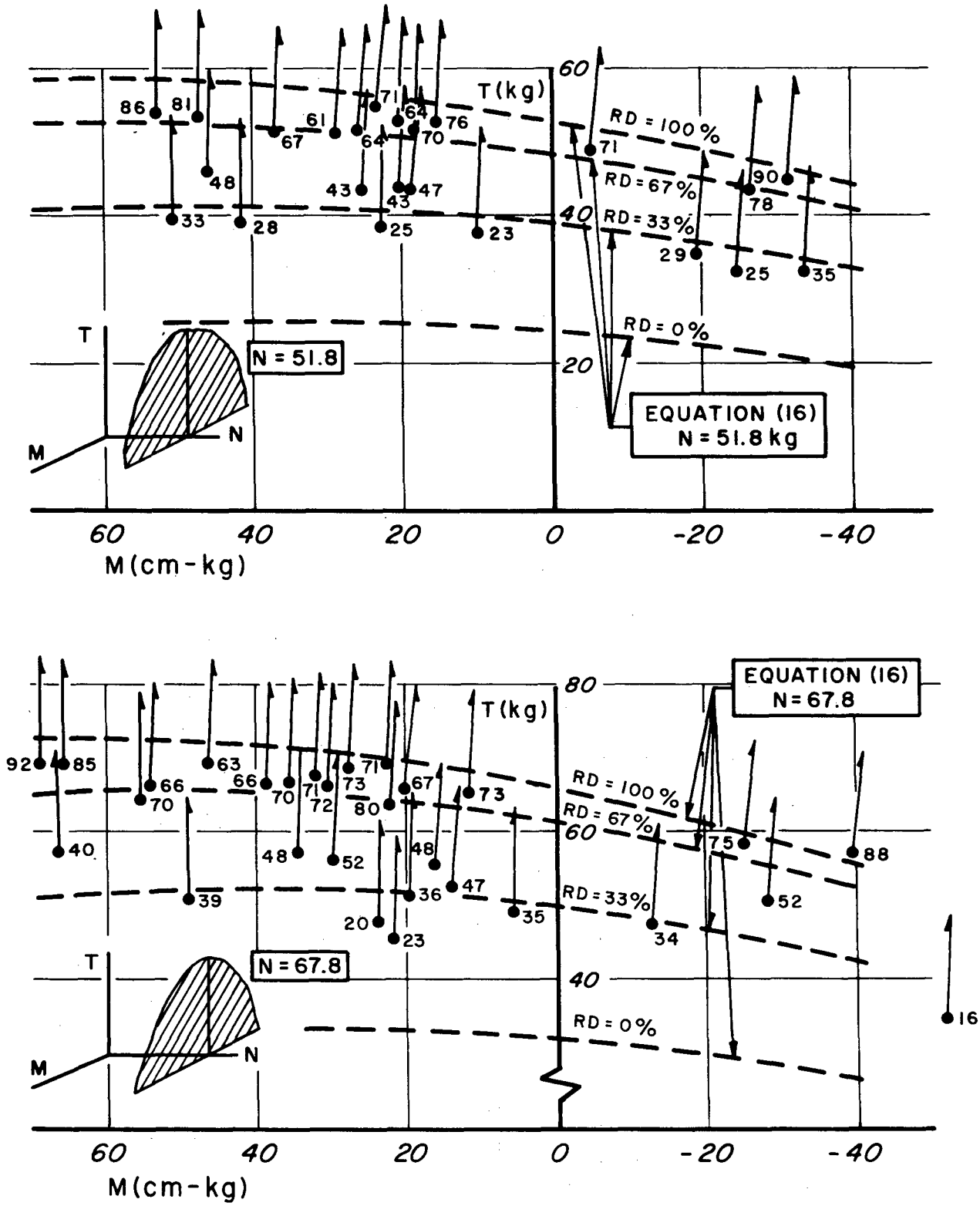


FIG. 12 PLOTS OF FAILURE FORCE COORDINATES AND DISPLACEMENT INCREMENT VECTOR PROJECTIONS FOR TESTS HAVING FINAL NORMAL LOADS OF 51.8 KG. AND 67.8 KG.

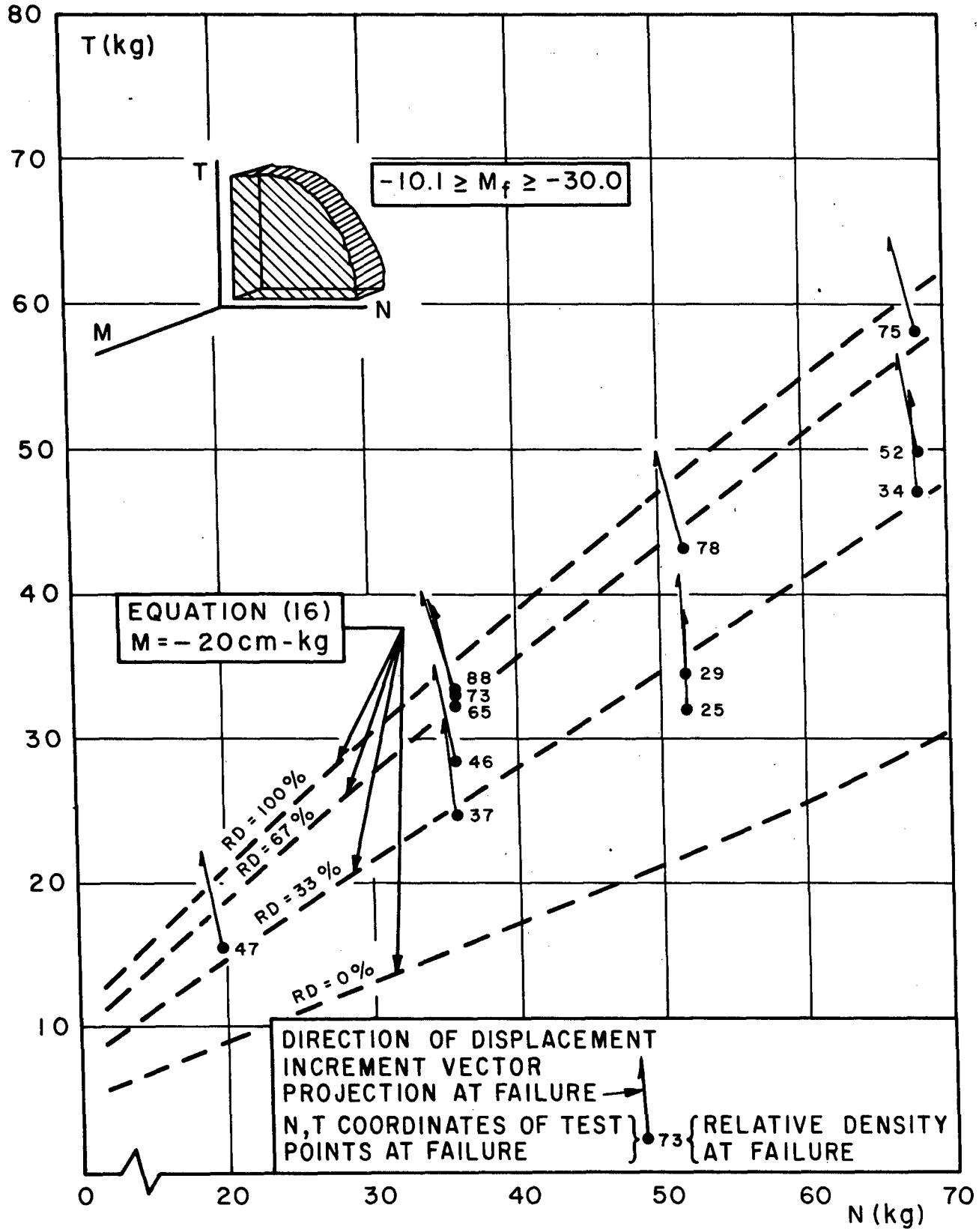


FIG. 13 PLOT OF FAILURE COORDINATES AND DISPLACEMENT INCREMENT VECTOR PROJECTIONS FOR TESTS HAVING A MOMENT AT FAILURE BETWEEN -10.1 CM.-KG. AND -30.0 CM.-KG.

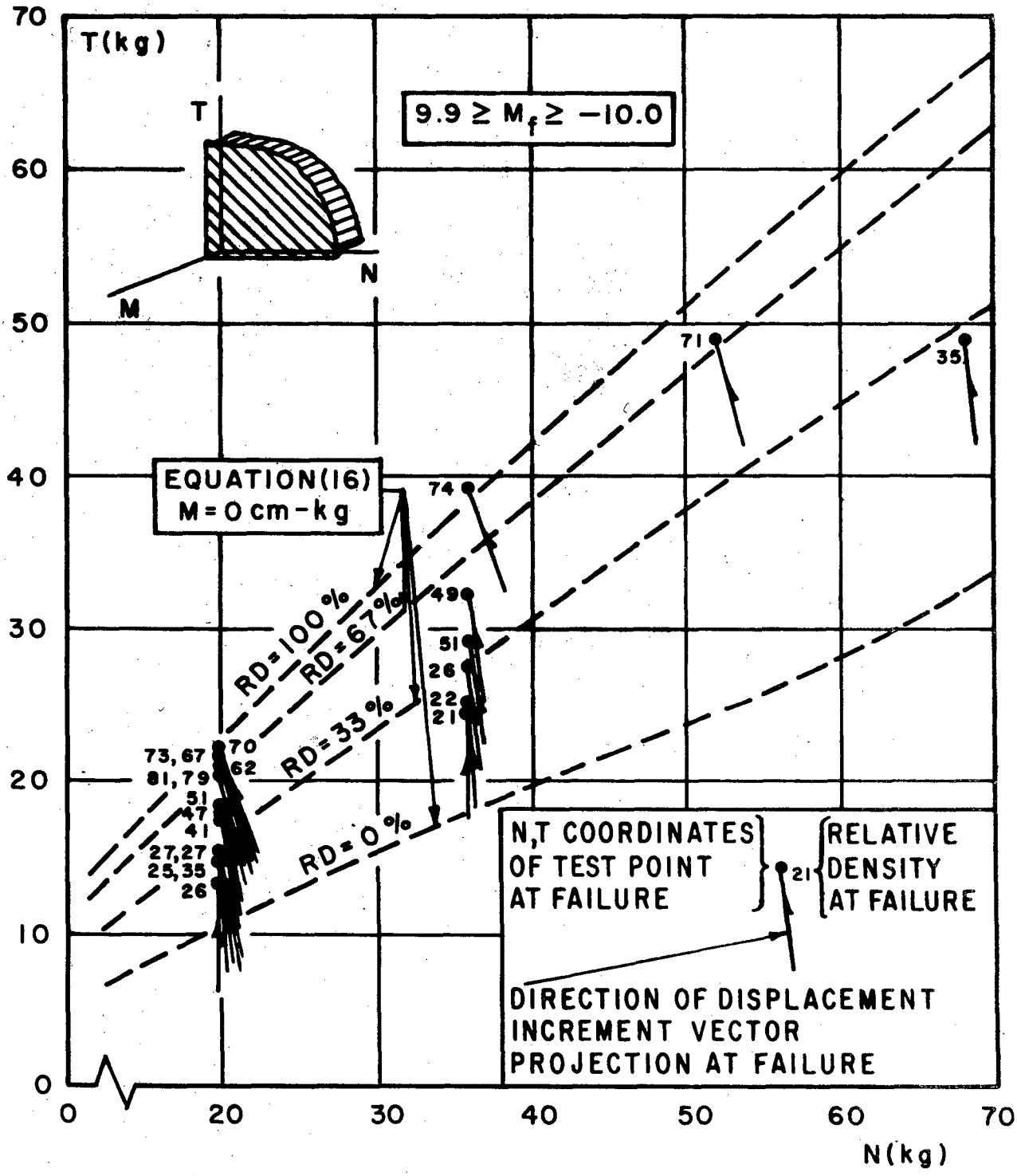


FIG. 14 PLOT OF FAILURE FORCE COORDINATES AND DISPLACEMENT INCREMENT VECTOR PROJECTIONS FOR TESTS HAVING A MOMENT AT FAILURE BETWEEN +9.9 CM.-KG. AND -10.0 CM.-KG.

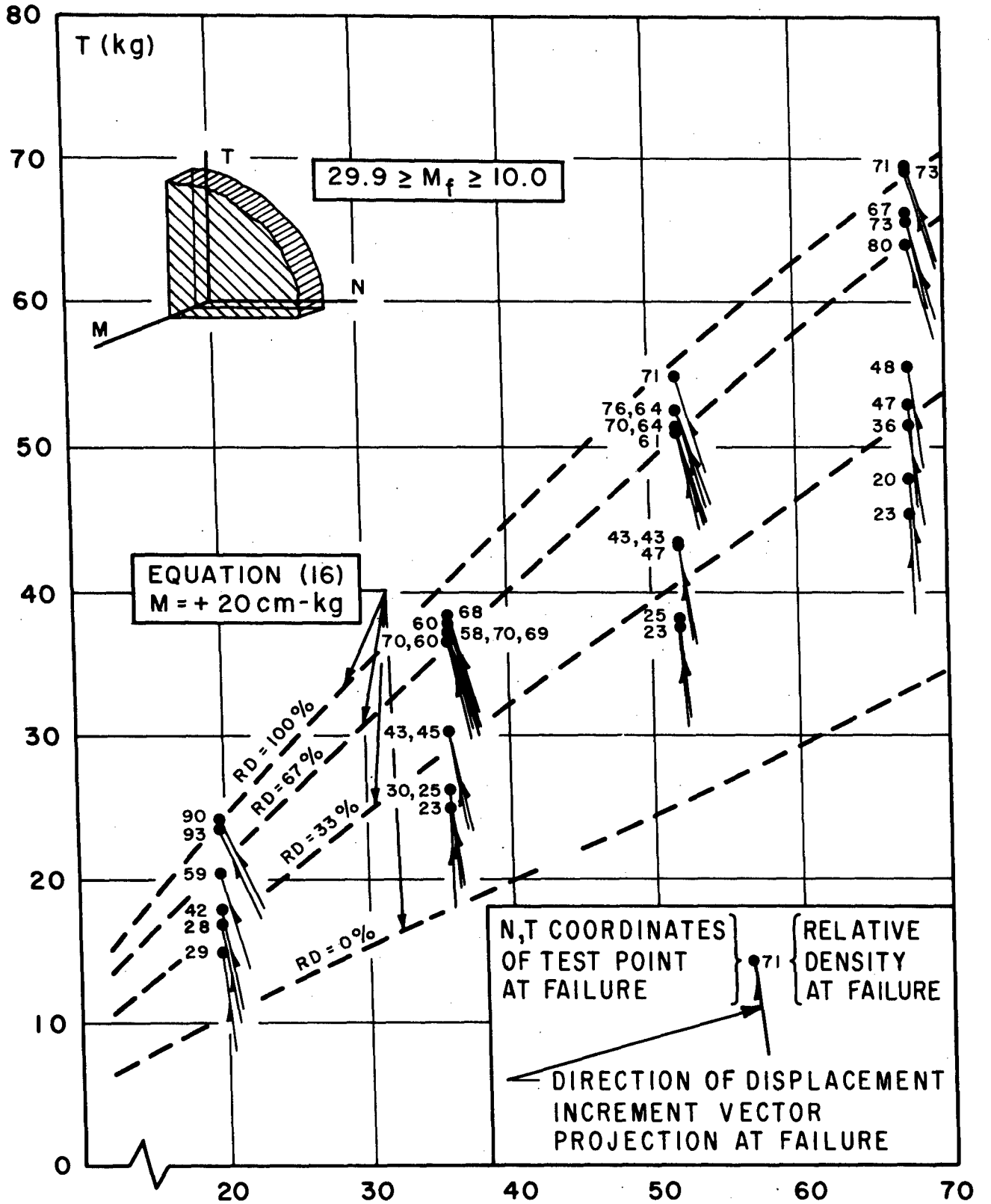


FIG. 15 PLOT OF FAILURE FORCE COORDINATES AND DISPLACEMENT INCREMENT VECTOR PROJECTIONS FOR TESTS HAVING A MOMENT AT FAILURE BETWEEN +29.9 CM.-KG. AND +10.0 CM.-KG.

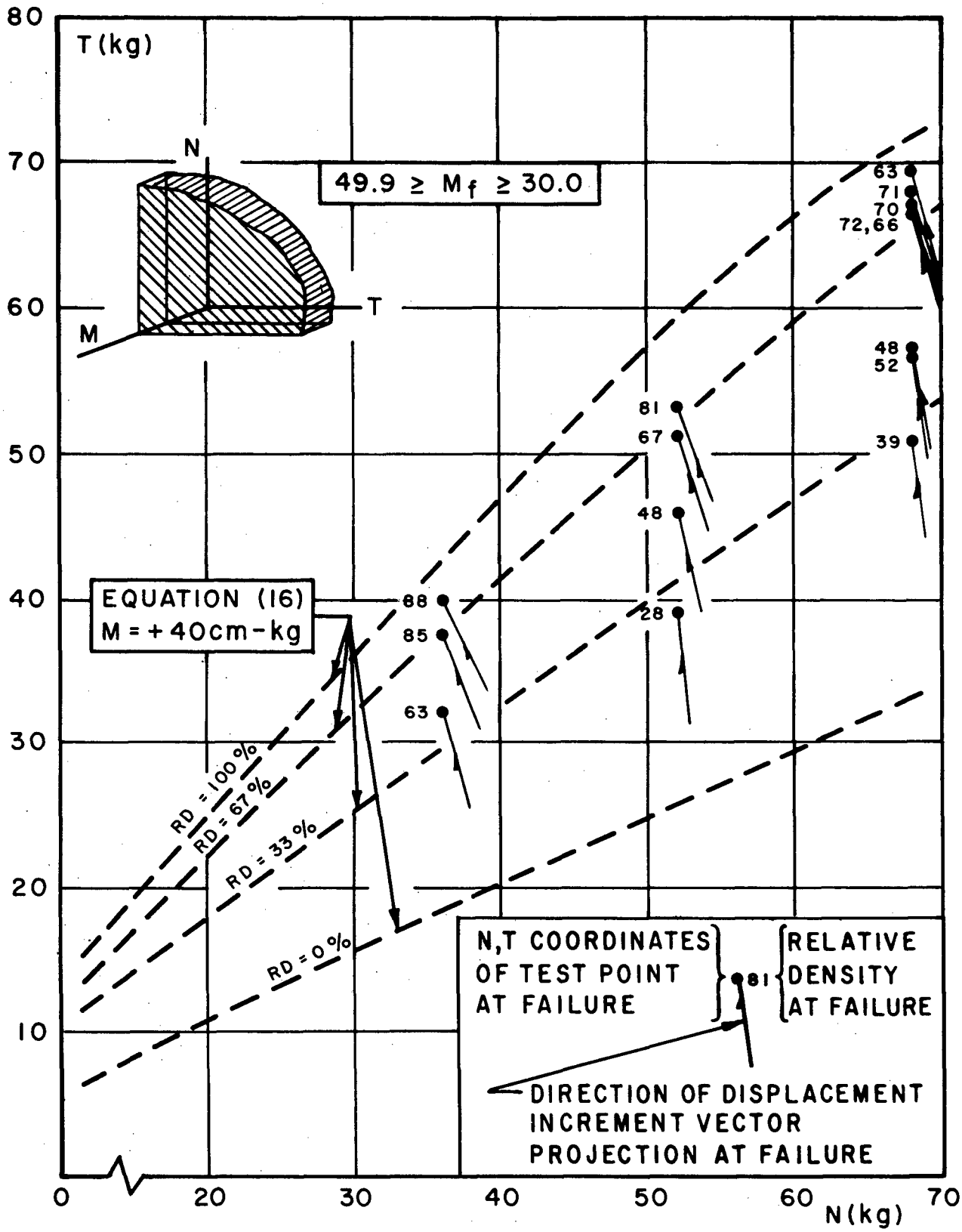


FIG. 16 PLOT OF FAILURE FORCE COORDINATES AND DISPLACEMENT INCREMENT VECTOR PROJECTIONS FOR TEST HAVING A MOMENT AT FAILURE BETWEEN +49.9 CM.-KG. AND +30.0 CM.-KG.

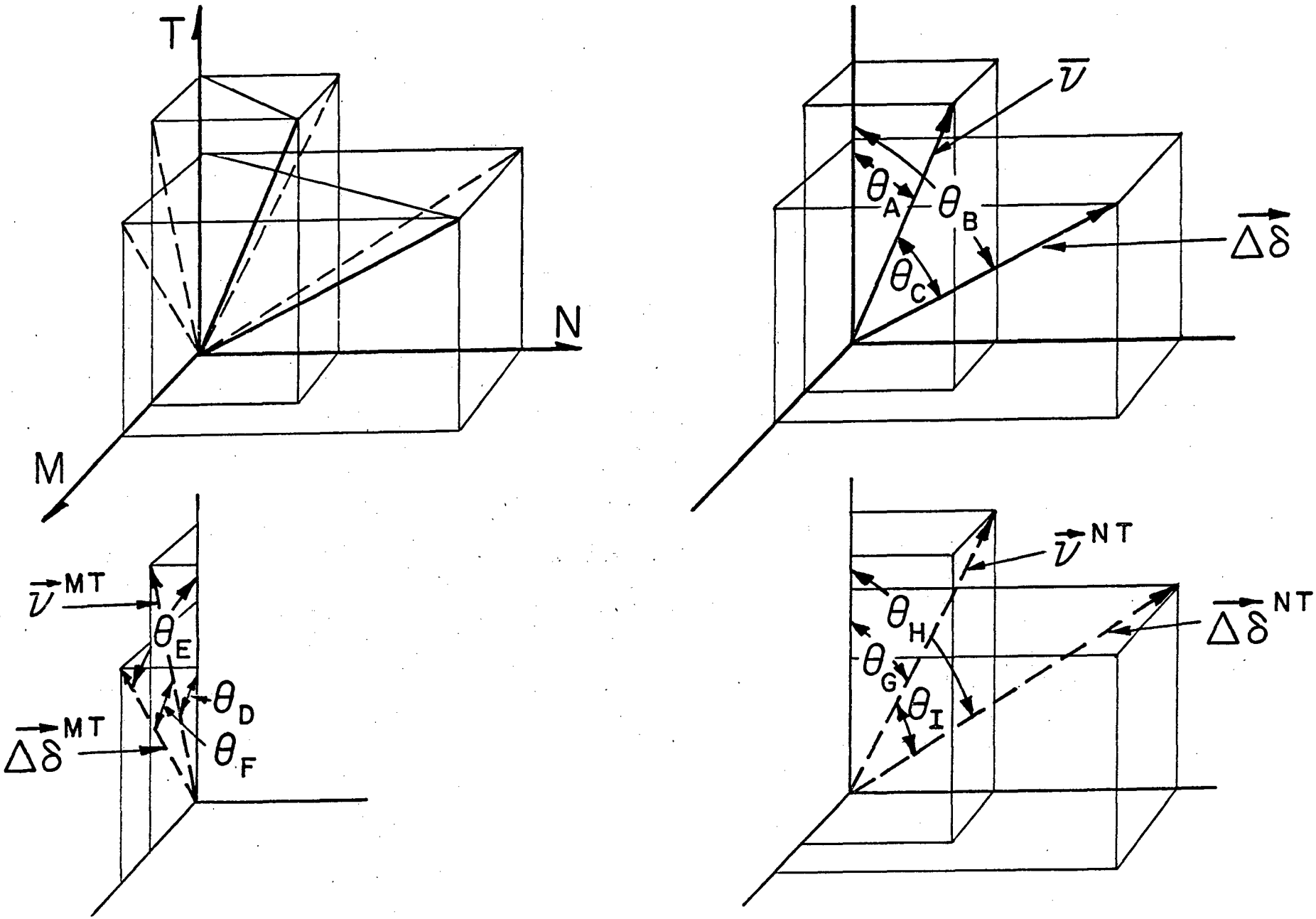


FIG. 17 PICTORAL IDENTIFICATION OF VECTORS AND ANGLES DEFINED BY EQUATIONS (19) THROUGH (21).

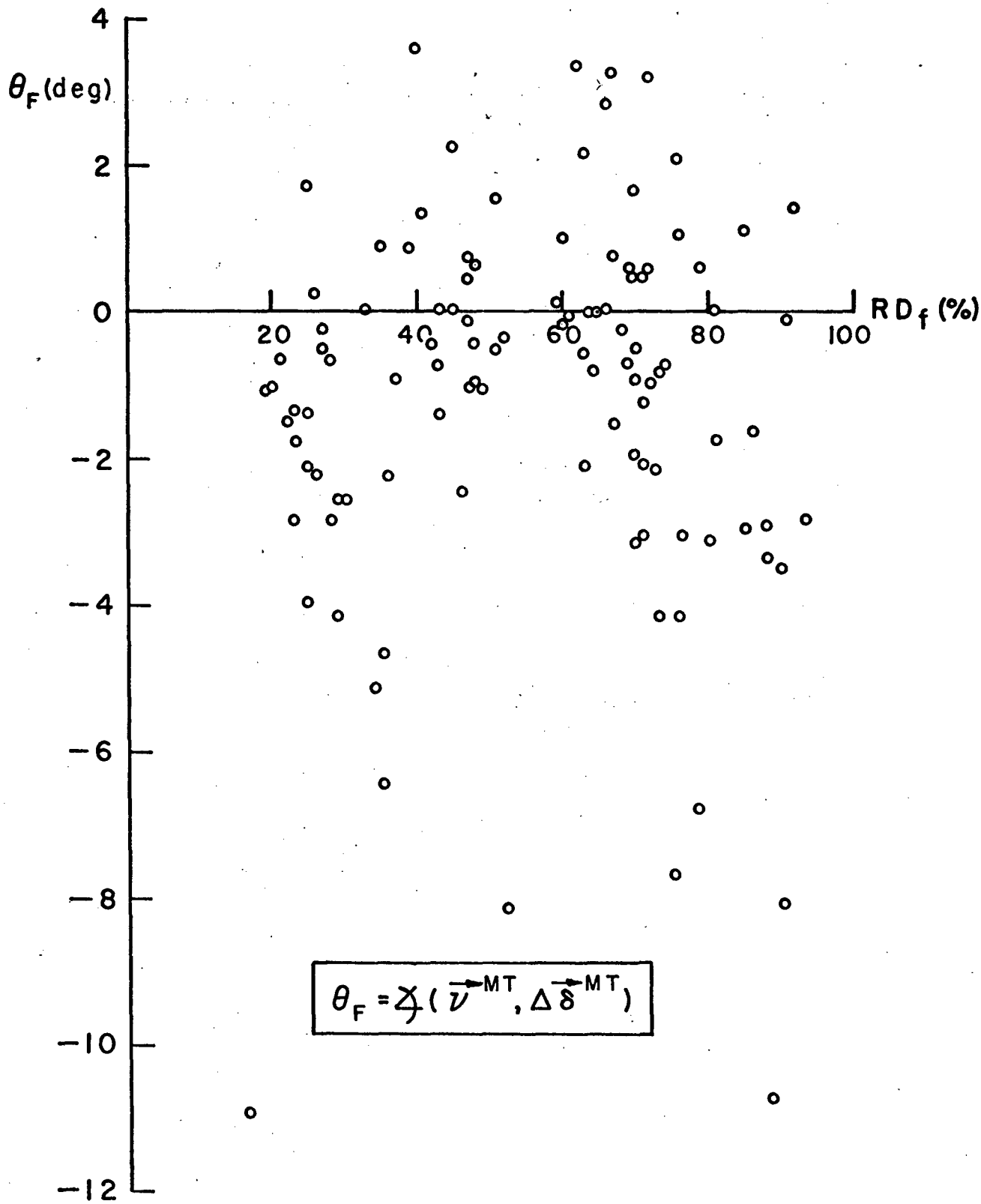


FIG. 18 SCATTER DIAGRAM OF THE ANGLE $\theta_F$ VERSUS THE RELATIVE DENSITY AT FAILURE.

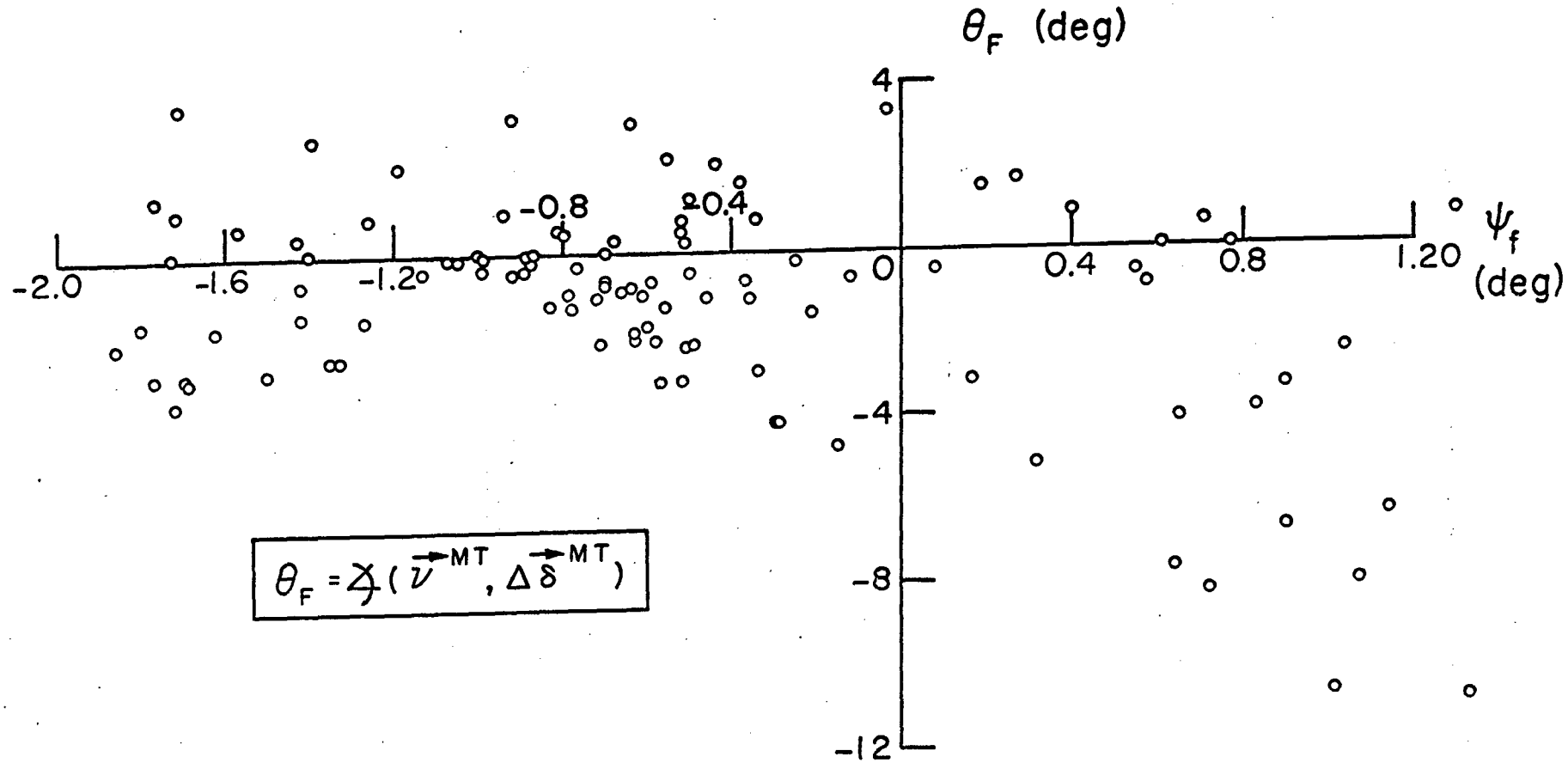


FIG. 19 SCATTER DIAGRAM OF THE ANGLE $\theta_F$ VERSUS THE ANGLE OF TILT AT FAILURE.

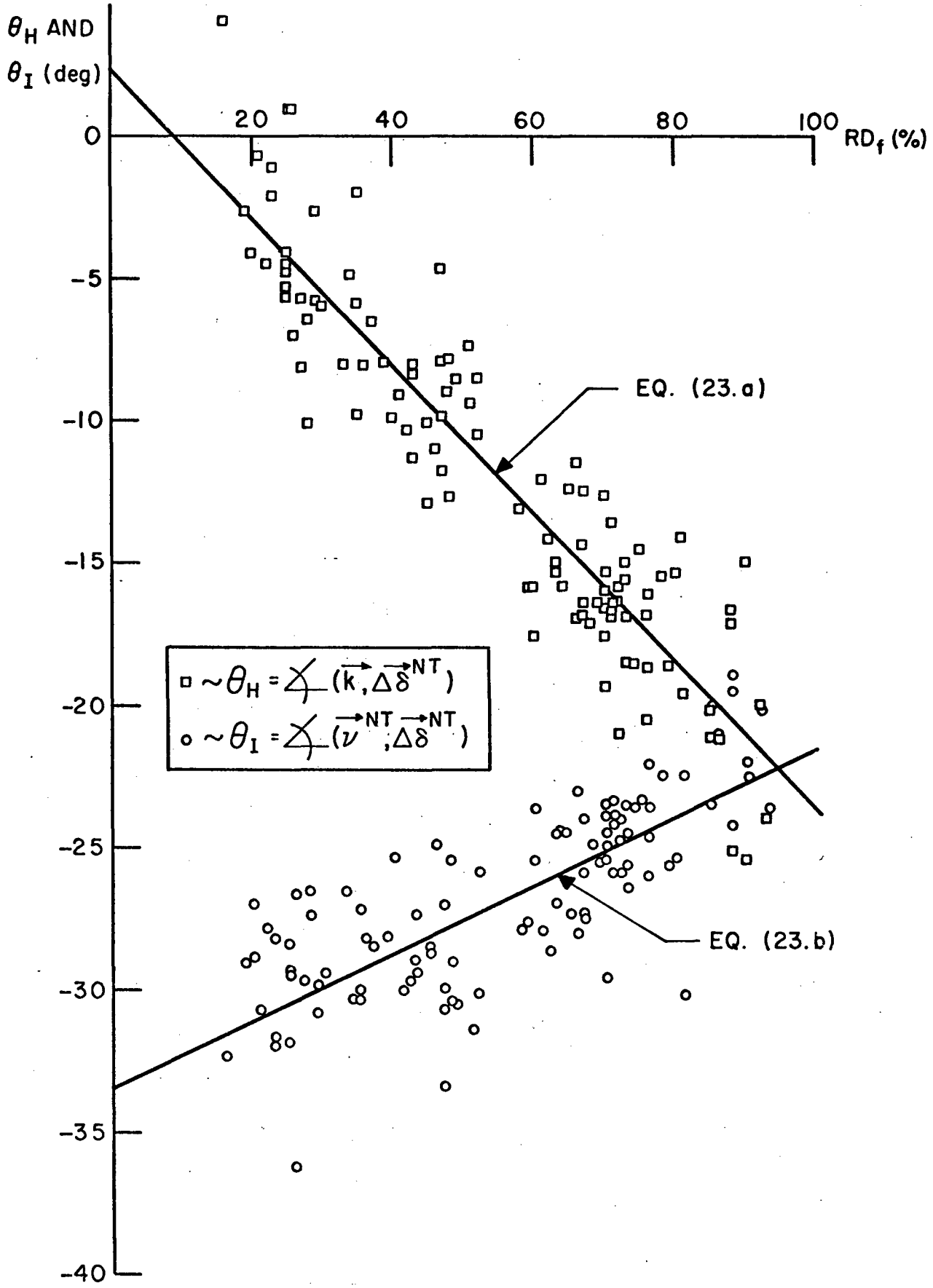


FIG. 20 SCATTER DIAGRAM OF THE ANGLES $\theta_H$ AND $\theta_I$ VERSUS THE RELATIVE DENSITY AT FAILURE.

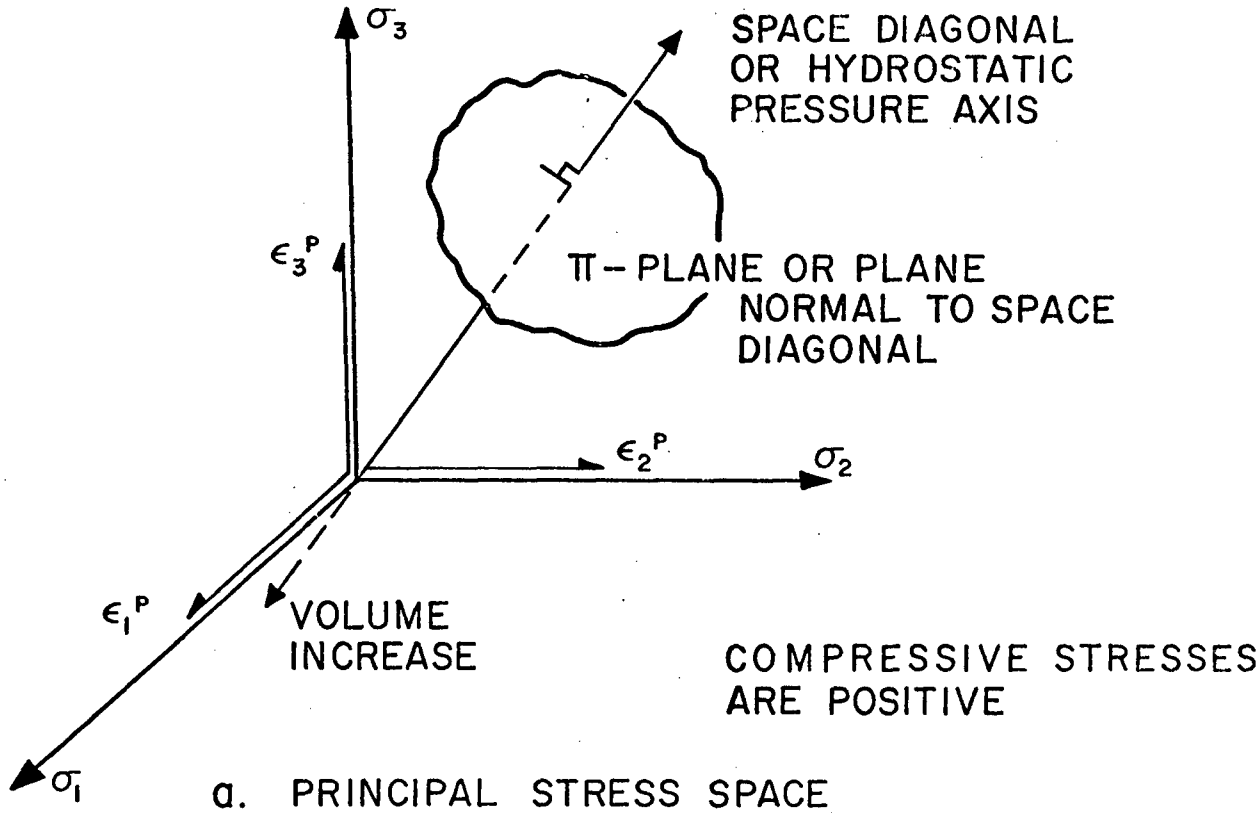


a. PRINCIPAL STRESS SPACE

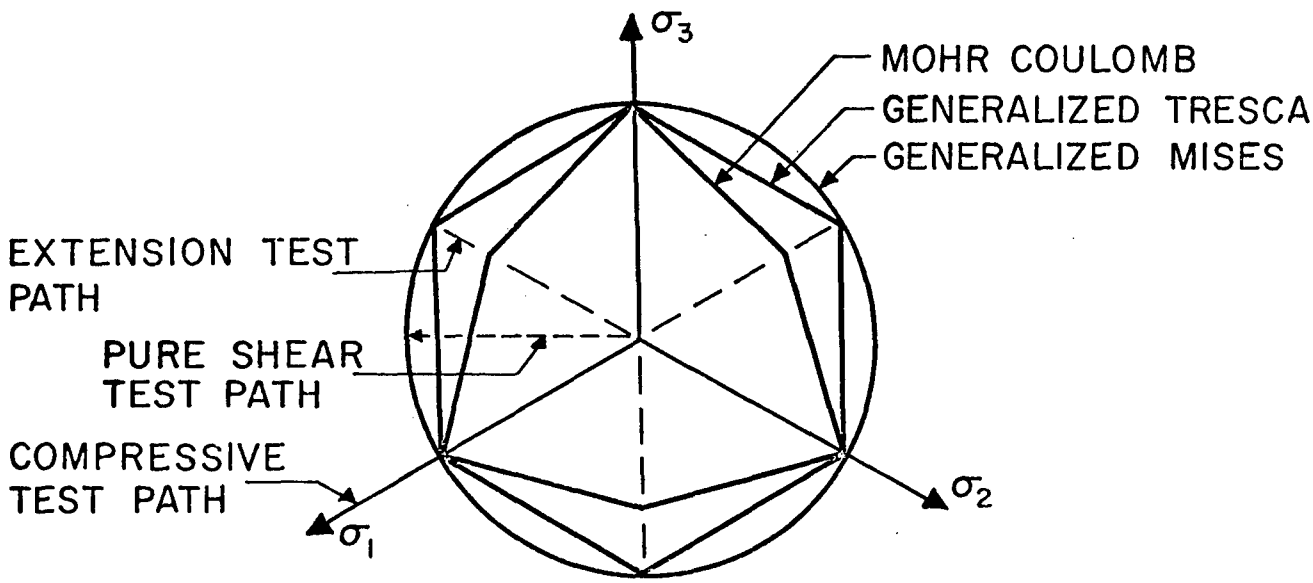


b. INTERSECTION OF TYPICAL ANALYTICAL FAILURE THEORIES WITH π PLANE

FIG. 21 PRINCIPAL STRESS SPACE AND FAILURE THEORIES.